EFFECT OF ELECTRIC FIELD ON MOLECULAR AND ELECTRONIC STRUCTURES OF GRAPHENE WITH 4N-DIVACANCY DEFECT AND APPLICATION ON HYDROGEN GAS STORAGE

Mr. Thanawit Kuamit

จุฬาลงกรณ์มหาวิทยาลัย
CHULALONGKORN UNIVERSITY

A Dissertation Submitted in Partial Fulfillment of the Requirements
for the Degree of Doctor of Philosophy in Chemistry
Department of Chemistry
FACULTY OF SCIENCE
Chulalongkorn University
Academic Year 2021
Copyright of Chulalongkorn University

ผลของสนามไฟฟ้าต่อโครงสร้างโมเลกุลและอิเล็กตรอนของแกรฟีนที่มีความบกพร่องโฟร์เอ็น-ไดวาแคนซีและการประยุกต์ด้านกักเก็บแก๊สไฮโดรเจน

นายธนาวิทย์ เกื้อมิตร

จุฬาลงกรณ์มหาวิทยาลัย
CHULALONGKORN UNIVERSITY

วิทยานิพนธ์นี้เป็นส่วนหนึ่งของการศึกษาตามหลักสูตรปริญญาวิทยาศาสตรดุษฎีบัณฑิต
สาขาวิชาเคมี ภาควิชาเคมี
คณะวิทยาศาสตร์ จุฬาลงกรณ์มหาวิทยาลัย
ปีการศึกษา 2564

ลิขสิทธิ์ของจุฬาลงกรณ์มหาวิทยาลัย

Thesis Title	EFFECT OF ELECTRIC FIELD ON MOLECULAR AND ELECTRONIC STRUCTURES OF GRAPHENE WITH 4N-DIVACANCY DEFECT AND APPLICATION ON HYDROGEN GAS STORAGE
By	Mr. Thanawit Kuamit
Field of Study	Chemistry
Thesis Advisor	Professor VUDHICHAI PARASUK, Ph.D.

Accepted by the FACULTY OF SCIENCE, Chulalongkorn University in Partial Fulfillment of the Requirement for the Doctor of Philosophy

..... Dean of the FACULTY OF SCIENCE
(Professor POLKIT SANGVANICH, Ph.D.)

DISSERTATION COMMITTEE

..... Chairman
(Assistant Professor VARAWUT TANGPASUTHADOL, Ph.D.)

..... Thesis Advisor
(Professor VUDHICHAI PARASUK, Ph.D.)

..... Examiner
(Assistant Professor SAKULSUK UNARUNOTAI, Ph.D.)

..... Examiner
(Assistant Professor NUMPON INSIN, Ph.D.)

..... External Examiner
(Chompoonut Rungnim, Ph.D.)

จุฬาลงกรณ์มหาวิทยาลัย
CHULALONGKORN UNIVERSITY

ธนาวิทย์ เกื้อมิตร : ผลของสนามไฟฟ้าต่อโครงสร้างโมเลกุลและอิเล็กตรอนของแกรฟีนที่มีความบกพร่องโฟร์เอ็น-ไดวาแคนซีและการประยุกต์ด้านกักเก็บแก๊สไฮโดรเจน. (EFFECT OF ELECTRIC FIELD ON MOLECULAR AND ELECTRONIC STRUCTURES OF GRAPHENE WITH 4N-DIVACANCY DEFECT AND APPLICATION ON HYDROGEN GAS STORAGE) อ.ที่ปรึกษาหลัก : ศ. ดร.วุฒิชัย พาราสุข

งานวิจัยนี้ได้ศึกษาผลกระทบของสนามไฟฟ้าภายนอก (External Electric Fields, EEFs) ต่อโครงสร้างและสมบัติทางอิเล็กทรอนิกส์ของแกรฟีนควอนตัมดอท (GQDs) และ แกรฟีนควอนตัมดอท ที่มีความบกพร่องชนิดโฟร์เอ็น-ไดวาแคนซี ที่เจือด้วยโลหะ (m-4N-GQDs) โดยวิธีทฤษฎีความหนาแน่น (Density Functional Theory, DFT) ด้วยฟังก์ชันนัล M06-2x และเบซิสเซท 6-31g (d) ในการศึกษานี้ทำภายใต้ช่วงสนามไฟฟ้าตั้งแต่ -0.035 ถึง 0.035 หน่วยอะตอม (atomic units, a.u.) โดยศึกษา GQDs ที่มีขนาดต่างกันสามขนาดได้แก่ $C_{24}H_{12}$, $C_{54}H_{18}$, และ $C_{96}H_{24}$ และโลหะที่เจือใน 4N-GQDs ประกอบด้วย Ca, Ca^{2+}, Cr, Cr^{2+} ,Fe และ Fe^{2+} ผลการศึกษายังเปิดเผยว่าความโค้งของ GQDs และ m-4N-GQDs ภายใต้สนามไฟฟ้าในทิศทางบวกและลบเป็นในทิศทางตรงข้ามกัน อีกทั้งความโค้งของ GQDs และ m-4N-GQDs เป็นสัดส่วนโดยตรงกับความแรงของสนามไฟฟ้า โดยเรียงลำดับตามความโค้งของ GQDs ได้ดังนี้ $C_{96}H_{24}$ > $C_{54}H_{18}$ > $C_{24}H_{12}$ ช่องว่าง HOMO-LUMO ขึ้นอยู่กับทั้งขนาดและสนามไฟฟ้า ช่องว่าง HOMO-LUMO ของ $C_{24}H_{12}$, $C_{54}H_{18}$ และ $C_{96}H_{24}$ คือ 5.87-5.90, 3.98-4.43 และ 2.43-3.31 eV ตามลำดับ นอกจากนี้ช่องว่างจะแตกต่างกันไปตามโลหะที่เจือใน 4N-GQDs เรียงลำดับดังนี้: Cr ≈ Fe > Ca > Ca^{2+} > Cr^{2+} ≈ Fe^{2+} ซึ่งช่องว่าง HOMO-LUMO อยู่ในช่วง 1.38 ถึง 2.98 eV นอกจากนี้เรายังพบว่าช่องว่าง HOMO-LUMO จะลดลงเมื่อมีความโค้งเพิ่มขึ้น ดังนั้นสมบัติทางอิเล็กทรอนิกส์ของ GQDs และ m-4N-GQDs แบบโค้งสามารถปรับเปลี่ยนได้โดยใช้สนามไฟฟ้า พิจารณาพลังงานการดูดซับของ H_2 บน Fe^{2+}-4N-GQDs ที่มีองศาความโค้งและตำแหน่งการดูดซับ H_2 ที่แตกต่างกันทั้งภายในและภายนอกโค้งของ Fe^{2+}-4N-GQDs พบว่าโมเลกุล H_2 ชอบดูดซับภายนอกโค้งของ Fe^{2+}-4N-GQDs โดยมีระยะห่างระหว่าง Fe^{2+} และ H_2 ที่ 3.0 – 3.5 Å (-2.03 ถึง -0.38 กิโลแคลอรี่/โมล) พลังงานการดูดซับ H_2 ในกรณีดูดซับภายนอกโค้งสัมพันธ์โดยตรงกับความแรงของสนามไฟฟ้า ในขณะที่ในกรณีดูดซับภายในโค้ง ค่าพลังงานดูดซับ H_2 มีค่าใกล้คียงกันกันไม่ขึ้นกับความแรงสนาม ดังนั้นการดูดซับ H_2 โมเลกุลสามารถถูกควบคุมด้วยความโค้งของ Fe^{2+}-4N-GQDs เราจึงสามารถใช้ Fe^{2+}-4N-GQDs แบบโค้งสำหรับการจัดเก็บก๊าซไฮโดรเจนได้

จุฬาลงกรณ์มหาวิทยาลัย
CHULALONGKORN UNIVERSITY

สาขาวิชา	เคมี	ลายมือชื่อนิสิต .....
ปีการศึกษา	2564	ลายมือชื่อ อ.ที่ปรึกษาหลัก .....

6072806023 : MAJOR CHEMISTRY

KEYWORD: External Electric Fields (EEFs), Graphene Quantum Dots (GQDs), metallo-4N-divacancy defect GQDs (m-4N-GQDs), HOMO-LUMO gap, Hydrogen Adsorption

Thanawit Kuamit : EFFECT OF ELECTRIC FIELD ON MOLECULAR AND ELECTRONIC STRUCTURES OF GRAPHENE WITH 4N-DIVACANCY DEFECT AND APPLICATION ON HYDROGEN GAS STORAGE. Advisor: Prof. VUDHICHAI PARASUK, Ph.D.

The effect of external electric fields (EEFs) on geometries and electronic properties of graphene quantum dots (GQDs) and m-4N-divacancy defect GQDs (m-4N-GQDs) was studied using density functional theory (DFT) method with M06-2x functional and 6-31g (d) basis set. An external electric field with strength ranging from -0.035 to 0.035 atomic units (a.u.) was applied normal to the molecular plane. Three different sizes, i.e., $C_{24}H_{12}$, $C_{54}H_{18}$, and $C_{96}H_{24}$, were investigated. The metal doping in m-4N-GQDs consists of Ca, Ca^{2+}, Cr, Cr^{2+}, Fe, and Fe^{2+}. Our results revealed that GQDs and m-4N-GQDs are curved under EEFs in the direction opposite to the applied field. The curvature of the GQDs and m-4N-GQDs is directly proportional to the electric field strength. The curvature of GQDs is in the following order: $C_{96}H_{24} > C_{54}H_{18} > C_{24}H_{12}$. The HOMO-LUMO gap depends on both size and EEFs. HOMO-LUMO gaps of $C_{24}H_{12}$, $C_{54}H_{18}$, and $C_{96}H_{24}$ are 5.87-5.90, 3.98-4.43, and 2.43-3.31 eV, respectively. In addition, the gap varies with the metal doping and the order is as following: Cr ≈ Fe > Ca > Ca^{2+} > Cr^{2+} ≈ Fe^{2+}. The HOMO-LUMO gap of m-4N-GQDs are in ranges from 1.38 to 2.98 eV. We also found the HOMO-LUMO gap to be decreased with the increase of the curvature. Therefore, the electronic properties of curved GQDs and m-4N-GQDs could be modified through EEFs. Moreover, the adsorption energies of H_2 on Fe^{2+}-4N-GQDs with different degrees of curvature and H_2 adsorption positions, inside or outside, of curved Fe^{2+}-4N-GQDs were studied. It was found that the molecular H_2 prefers to adsorb outside of curved Fe^{2+}-4N-GQDs, which have a distance between Fe^{2+} and H_2 at 3.0 – 3.5 Å (-2.03 to -0.38 kcal/mol). The adsorption energy at outside H_2 adsorption is directly related to the electric field strength, while inside H_2 adsorption is similar. The curved Fe^{2+}-4N-GQDs could control molecular H_2 adsorption. The curved Fe^{2+}-4N-GQDs can be applied for hydrogen gas storage.

Field of Study:	Chemistry	Student's Signature .....
Academic Year:	2021	Advisor's Signature .....

ACKNOWLEDGEMENTS

This study was carried out in the Chemistry Department, Faculty of Science, Chulalongkorn University.

I would like to express my special gratitude to my advisor, Professor Dr. Vudhichai Parasuk, for providing me with all the necessary facilities. In addition, he should please help me and give valuable advice throughout the course of my studies.

I also would like to thank Assistant Professor Dr. Varawut Tangpasuthadol, Assistant Professor Dr. Sakulsuk Unarunotai, Assistant Professor Dr. Numpon Insin, and Dr. Chompoonut Rungnim for their kind attention and helpful suggestions on my thesis committee.

I would like to acknowledge the 90th anniversary of Chulalongkorn University for Mr. Thanawit Kuamit's scholarship. Additionally, I'm grateful for computational resources supported by the Center of Excellence in Computational Chemistry (CECC), Department of Chemistry, Chulalongkorn University, the National Electronics and Computer Technology Center (NECTEC) under the National e-Science Consortium, and the NSTDA Supercomputer Center (ThaiSC) for this work.

Thanawit Kuamit

จุฬาลงกรณ์มหาวิทยาลัย
CHULALONGKORN UNIVERSITY

TABLE OF CONTENTS

Page

ABSTRACT (THAI) iii

ABSTRACT (ENGLISH) iv

ACKNOWLEDGEMENTS v

TABLE OF CONTENTS vi

LIST OF FIGURES viii

LIST OF TABLES x

CHAPTER I INTRODUCTION 1

1.1 RESEARCH OBJECTIVES 4

CHAPTER II THEORHYTICAL BACKGROUND 5

2.1 THE SCHRÖDINGER EQUATION 5

2.2 HARTREE-FOCK (HF) APPROXIMATION 6

2.3 DENSITY FUNCTIONAL THEORY 8

2.4 BASIS SET 11

2.4.1 Slater type atomic orbitals 11

2.4.2 Gaussian type atomic orbitals 11

2.4.3 Types of basis sets 12

2.4.3.1 Minimal basis sets 12

2.4.3.2 Extended basis sets 12

Split-Valence 12

Polarized basis sets 13

CHAPTER III DETAILS OF THE CALCULATION 14

จุฬาลงกรณ์มหาวิทยาลัย
Chulalongkorn University

3.1 COMPUTATIONAL METHOD 14

3.2 GEOMETRIES OF GQDS 14

3.3 GEOMETRIES OF m-4N-GDQs 15

3.4 H_2-ADSORPTION ON CURVED Fe^{2+}-4N-GDQS 17

CHAPTER IV RESULTS AND DISCUSSION 18

4.1 THE EFFECT OF EXTERNAL ELECTRIC FIELD ON MOLECULAR STRUCTURE 18

4.1.1 CURVING OF GQDs BY EEFSs 18

4.1.2 CURVING OF m-4N-GQDs BY EEFSs 23

4.2 THE EFFECT OF EXTERNAL ELECTRIC FIELD ON ELECTRONIC PROPERTY 30

4.2.1 THE EFFECT OF EEFSs ON HOMO-LUMO GAP OF GQDs 30

4.2.2 THE EFFECT OF EEFSs ON HOMO-LOMO GAP OF 4m-4N-GQDs 32

4.3 THE ADSORPTION OF MOLECULAR H_2 ON CURVED Fe^{2+}-4N-GQDs 35

CHAPTER V CONCLUSION 39

REFERENCES 40

APPENDIX 46

VITA 55

จุฬาลงกรณ์มหาวิทยาลัย
CHULALONGKORN UNIVERSITY

LIST OF FIGURES

Page

Figure 1 Model of graphene sheet..... 1

Figure 2 The geometry of (a) $C_{24}H_{12}$, (b) $C_{54}H_{18}$, and (c) $C_{96}H_{24}$ and the direction of the applied field..... 15

Figure 3 Two curving directions, along C atoms and C-C bond directions, of (a) $C_{24}H_{12}$, (b) $C_{54}H_{18}$, and (c) $C_{96}H_{24}$..... 15

Figure 4 Schematic of the metal-4N-GDQs models (metal; Ca, Ca^{2+}, Cr, Cr^{2+}, Fe, and Fe^{2+})..... 16

Figure 5 Two curving directions, along C atoms and C-C bond directions, m-4N-GQDs. 16

Figure 6 The adsorption of H_2 on curved Fe^{2+}-4N-GDQs with various degrees of curvature, a) = 0, b) = -0.00728 c) = -0.01694, d) = -0.04018 e) = -0.06512, f) = -0.08139, g) = -0.0915, e) = 0.00728, f) = 0.01694, g) = -0.04018., k) = 0.06512, l) = 0.08139, m) = 0.0915. 17

Figure 7 Geometries optimization of GDQs model, of (A) $C_{24}H_{12}$, (B) $C_{54}H_{18}$, and (C) $C_{96}H_{24}$, with different electric fields, a) = 0.0 a.u., b) = 0.010 a.u., c) = 0.0150 a.u., d) = 0.020 a.u., e) = 0.025 a.u., f) = 0.030 a.u. g) = 0.035 a.u..... 19

Figure 8 Dependent of the degree of curvature on external electric field for $C_{24}H_{12}$, $C_{54}H_{18}$, and $C_{96}H_{24}$. 21

Figure 9 Geometries optimization of m-4N-GDQs model, of (A) Ca, (B) Cr, and (C) Fe, with different electric fields, a) = 0.0 a.u., b) = 0.010 a.u., c) = 0.0150 a.u., d) = 0.020 a.u., e) = 0.025 a.u., f) = 0.030 a.u. g) = 0.035 a.u..... 24

Figure 10 Geometries optimization of m-4N-GDQs model, of (A) Ca^{2+}, (B) Cr^{2+}, and (C) Fe^{2+}, with different electric fields, a) = 0.0 a.u., b) = 0.010 a.u., c) = 0.0150 a.u., d) = 0.020 a.u., e) = 0.025 a.u., f) = 0.030 a.u. g) = 0.035 a.u..... 25

Figure 11 Dependent of the degree of curvature on external electric field for m-4N-GDQs. 26

Figure 12 Calculated the different an electric fields and the HOMO-LUMO gap energies of $C_{24}H_{12}$, $C_{54}H_{18}$, and $C_{96}H_{24}$. 31

Figure 13 The degree of curvature |a|, fitted by a quadratic equation, and the HOMO-LUMO gap energies of $C_{24}H_{12}$, $C_{54}H_{18}$, and $C_{96}H_{24}$. 31

Figure 14 Calculated the different an electric fields and the HOMO-LUMO gap energies of m-4N-GDQs. 33

Figure 15 The degrees of curvatures |a|, fitted by a quadratic equation, and the HOMO-LUMO gap energies of m-4N-GDQs. 34

Figure 16 Side view single point calculation of Fe^{2+}-4N-GDQs adsorbed H^2 with various degrees of curvature, a) = 0, b) = -0.00728 c) = -0.01694, d) = -0.04018 e) = -0.06512, f) = -0.08139, g) = -0.0915, e) = 0.00728, f) = 0.01694, g) = -0.04018., k) = 0.06512, l) = 0.08139, m) = 0.0915. 36

Figure 17 Adsorption energy, and distance between Fe^{2+} and H_2 center from 2.5 Å to 4.0 Å of Fe^{2+}-4N-GDQs adsorbed H_2 with different degrees of curvature (a) 38

จุฬาลงกรณ์มหาวิทยาลัย
CHULALONGKORN UNIVERSITY

LIST OF TABLES

Page

Table 1 Dipole moment of $C_{24}H_{12}$, $C_{54}H_{18}$, and $C_{96}H_{24}$ under external electric fields from -0.035 to +0.035 a.u. 22

Table 2 Dipole moment of Ca, Cr and Fe-4N-GDQs under external electric fields from -0.035 to +0.035 a.u. 28

Table 3 Dipole moment of Ca^{2+}, Cr^{2+}, and Fe^{2+}-4N-GDQs under external electric fields from -0.035 to +0.035 a.u.. 29

Table 4 Adsorption energy, and distance between Fe^{2+} and H_2 center from 2.5 Å to 4.0 Å of Fe^{2+}-4N-GDQs adsorbed H_2 with different degrees of curvature (a)..... 37

จุฬาลงกรณ์มหาวิทยาลัย
CHULALONGKORN UNIVERSITY

CHAPTER I
INTRODUCTION

Graphene is a monolayer of carbon atoms arranged in the form of a two-dimensional and a hexagonal lattice, which is composed of a single atomic layer of graphite. **Figure 1**. It was isolated and characterized for the first time in 2004 by Andre Geim and Konstantin Novoselov at the University of Manchester.[1] Layers of graphene pull from graphite and transfer them onto thin Si/SiO_2 substrates, a process called micromechanical cleavage or "the Scotch tape method".

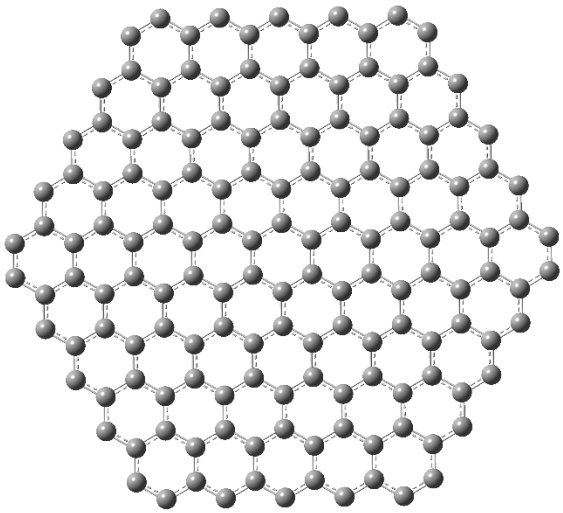

Figure 1 Model of graphene sheet

จุฬาลงกรณ์มหาวิทยาลัย
CHULALONGKORN UNIVERSITY

There are many reasons why graphene is of special interest to fundamental science because of the unique combination of its properties: light-weight composite, excellent electrical, extremely high surface area, and good thermal properties, etc. It has a variety of applications, such as solar cells[2], nanoelectronics devices[3], and hydrogen adsorption[4]. In this work, we are particularly interested in the applications of graphene as a nanoelectronics device and hydrogen adsorption.

Graphene quantum dots (GQDs), a single or a few layers of a nano-sized graphene sheet (less than 10 nm), have received much attention in various applications.[5-9] The fabrication of GQDs can be classified into two categories: top–down and bottom–up methods. The top-down approach is to cut down large

graphene sheets into small pieces of graphene sheet. Until now, for top–down approaches, electrochemical exfoliation, ultrasonication exfoliation, acidic oxidation, electron beam lithography, or chemical exfoliation have been used to synthesize GQDs. In the strategy of the bottom-up approach, small molecules are used as starting materials to produce GQDs. The bottom–up methods, using poly–cyclic aromatic compounds or the pyrolysis/carbonization of molecules with the aromatic structures as starting materials through stepwise microwave, hydrothermal, solvothermal, or template methods, have been utilized to prepare GQDs.[10-11]

In the manufacturing industry, graphene has frequently been used as a raw material for semiconductor and nanoelectronic devices owing to its excellent properties. These processes are usually deformed. The deformation of graphene can modify its electronic properties, which has recently attracted much attention.[12-16] Shen-Lin Chang et al.[17] reported that the increase in the arc angle of the curved armchair graphene nanoribbons leads to large changes in their electronic structure.

Pattarapongdilok et al.[18] suggested that the HOMO-LUMO gap of graphene quantum dots (GQDs) decreases when the degree of folding is increased to perform the density functional theory (DFT) calculations.

This concept could be used to construct GQDs-based electronic devices. The curving and bending of graphene affects its electronic properties. Various fabrication methods, such as AFM tip[19], mechanical exfoliation[20], chemical oxidation followed by thermal treatment[21], and printing[22], are used to fabricate the curving and bending of graphene. Bao et al.[23] investigated whether thermomechanical manipulation could control the dimensional periodic ripples in suspended graphene sheets. Graphene bubbles deposited on a substrate. It is possible to control the curvature of graphene by applying electric fields.[24] Zhang et al. suggest that the bending behaviors of graphene nanoribbons (GNRs) are enhanced by the surface adsorption of small molecules. The effect of small liquid droplets can induce a significant bending of the graphene surface.[25]

In recent years, there has been an increasing interest in the investigation of vacancy defects in graphene. The effect of different vacancy defects in graphene, such as Stone-Wales defects[26], Single vacancy defect[27], Multiple vacancy defects[28], and substitutional impurities[29-31], could change the mechanical properties as well as the electrical conductivities and thermal properties of graphene.

Nowadays, nitrogen doping in graphene has been an effective way to tailor the properties of graphene and extend its applications, such as catalysis[32], batteries[33], hydrogen storage materials[34], semiconductors[35], etc. Many synthesis methods have shown that nitrogen doping can be synthesized most generally by the chemical vapor deposition method, which contains different doping defect structures, such as one nitrogen atom substituted for a C atom, three nitrogen atoms around a vacancy, and four nitrogen atoms around a divacancy. We focused on metallo-4N-divacancy defect GQDs due to the fact that high anionic ligands can gain greater electrostatic stabilization when interacting with metal cations.[36]

Mombr et al.[37] fabricated a study to understand the consequences of vacancies with different configurations in graphene. The 1–8 order carbon vacancy systems for a particular terminal substitution were considered. The results show that graphene with various vacancies can be presented in different deformations. Moreover, the carbon vacancy degree possibly modified the electronic properties of graphene, which was used as a donor material in organic solar cells.[38]

Because graphene quantum dots (GQDs) and quantum dots with vacancy defects can be guided to curve, graphene curvature causes a significant change in electronic properties, such as HOMO-LUMO gap energy. Our research question is how to control the curvature of graphene quantum dots (GQDs) and with graphene quantum dots vacancy defects doped with metal (m-4N-GQDs).

On the other hand, multifarious studies have been carried out on hydrogen storage with the development of the automotive industry. One of the most promising materials that has attracted considerable attention is using two-dimensional (2D) carbonaceous and graphene materials as hydrogen storage. The hydrogen adsorption on pristine graphene is very low, so it cannot be stably adsorbed on graphene.[39-40] Several researchers recently proposed that transition-

metal atoms embedded in vacancy graphene can improve the interaction of doping atoms and hydrogen molecules.[41-44]

However, the molecular H_2 adsorption on curved m-4N-GQDs has not yet been studied. A research question is how to control molecular H_2 adsorption on curved Fe^{2+}-4N-GQDs with different degrees of curvature.

Moreover, GQDs and m-4N-GQDs could have a significant effect on electric field interaction, leading to probably controlling the curvature and electronic properties. The molecular H_2 adsorption can be turned by curved Fe^{2+}-4N-GQDs with different degrees of curvature.

1.1 RESEARCH OBJECTIVES

In this study, the effects of external electric fields on the geometry and electronic properties of GQDs and m-4N-GQDs were investigated. The electric fields from -0.035 to +0.035 a.u. were applied. In addition, the adsorption energies of H_2 molecules adsorbed on different degrees of curved Fe^{2+}-4N-GQDs were studied.

จุฬาลงกรณ์มหาวิทยาลัย
CHULALONGKORN UNIVERSITY

CHAPTER II
THEORHYTICAL BACKGROUND

The fundamentals of quantum chemistry are based on the laws of physics. In the principle of quantum chemistry, the Schrödinger's equation is solved to obtain the information involving between electrons and nuclei. Thus, it can be used to explain molecular behavior and properties of molecules. Computational quantum chemistry is typically separated into wave function-based (semi-empirical and ab initio) and density-based (density functional theory) approaches.

2.1 THE SCHRÖDINGER EQUATION

The Schrödinger equation [45] is defined as

$$\hat{H}\Psi = E\Psi \tag{2.1}$$

Where, H is the Hamiltonian operator, Ψ is the wave function, and E is the energy of the state.

The total Hamiltonian of a molecular system can be written in its most general form (all given in atom unit) as

จุฬาลงกรณ์มหาวิทยาลัย
CHULALONGKORN UNIVERSITY

$$H = T_N + T_e + V_{Ne} + V_{ee} + V_{NN} \tag{2.2}$$

where, T_N = nuclear kinetic term,

$$= \sum_A -\frac{1}{2M_A}\nabla_A^2 ,$$

T_e = electron kinetic term,

$$= \sum_i -\frac{1}{2}\nabla_i^2 ,$$

V_{Ne} = electron-nuclear attraction term,

$$= \sum_A \sum_i \frac{Z_A}{|\vec{R}_A - \vec{r}_j|},$$

V_{ee} = electron-electron repulsion term,

$$= \sum_{i<j} |\vec{r}_i - \vec{r}_j|^{-1}$$

and V_{NN} = nuclear -nuclear repulsion term,

$$= \sum_{A<B} \frac{Z_A Z_B}{|\vec{R}_A - \vec{R}_B|}.$$

with large dimensionality, solving the Schrödinger equation is too complicated. To reduce the complexity, the Born-Oppenheimer approximation, where the motion of the atomic nuclei and electron is separated, is assumed. Thus,

$$H_{elec} = T_e + V_{Ne} + V_{ee} \tag{2.3}$$

and

$$H_{elec}\Psi_{elec}(\vec{r};\vec{R}) = E_{elec}\Psi_{elec}(\vec{r};\vec{R}) \tag{2.4}$$

$\Psi_{elec}(\vec{r},\vec{R})$ is the electronic wave function which is the function of both the nuclear and electronic coordinates $(\vec{r})$. E_{elec} and parameterized by the molecular coordinate $(\vec{r})$ energy E_{total} is

$$E_{total} = E_{elec} + V_{NN} \tag{2.5}$$

2.2 HARTREE-FOCK (HF) APPROXIMATION

The electron-electron repulsion term(V_{ee}) makes it impossible to find an exact solution to the (2.4) equation.

In the HF approximation, the electron-electron repulsion is compromised by the mean-field approximation. The Hartree-Fock energy E_{HF} can then be expressed by

$$E_{HF} = \langle \Psi_0 | H_{el} | \Psi_0 \rangle \qquad (2.6).$$

$\Psi_0\rangle$ is the HF wave functions or the Slater determinant

$$= \frac{1}{\sqrt{N!}} \begin{pmatrix} \chi_1(\vec{x}_1)\chi_1(\vec{x}_1) & \cdots & \chi_N(\vec{x}_1) \\ \chi_1(\vec{x}_2)\chi_2(\vec{x}_2) & & \chi_N(\vec{x}_2) \\ \vdots & \ddots & \vdots \\ \chi_1(\vec{x}_N)\chi_2(\vec{x}_N) & \cdots & \chi_N(\vec{x}_N) \end{pmatrix} \qquad (2.7)$$

where $\chi_j(\vec{x}_1)$ = molecular orbital = $\chi_j(\vec{r}_i, \vec{w}_i)$

$\vec{x}_i$ = spatial-spin coordinate

$\vec{r}_i$ = spatial coordinate

$\vec{w}_i$ =spin coordinate

$\chi_j(\vec{x}_1)$ can be obtained through Fock equation below:

$$f\chi_i = \varepsilon_i \chi_i \text{ , i = 1, 2,..., N} \qquad (2.8)$$

where $\hat{f}$ is the Fock operater and ε_i is the orbital energy.

In which,

$$f = -\frac{1}{2}\nabla_i^2 - \sum_A^N \frac{Z_A}{ri_A} + V_{HF}(i) \qquad (2.9)$$

$$= h(i) + V_{HF}(i)$$

($h(i)$) = core-Hamiltonian

and $V_{HF}(i)$ = field potential

By introduction of basis-function, equation (2.8) can be translated in matrix from known as Roothan-Hall equation[46-47]:

$$\mathbb{F}\boldsymbol{c} = \mathbb{S}\boldsymbol{c}\mathbb{E} \tag{2.10}$$

where $\mathbb{F}$ = Fock matrix, $\mathbb{S}$= overlap matrix, and $\boldsymbol{c}$ = matrix of MO coefficient. In term of orbital, the Hartree-Fock energy is

$$E_{HF} = \sum_{a}[a|h|a] + \frac{1}{2}\sum_{a}\sum_{b}[aa|bb] - [ab|ab] \tag{2.11}$$

The first term in (2.11) is one-electron integral and the second term is two-electron integrals (coulomb and exchange, respectively)

The HF approximation describes the Fermi hole (correlation between electrons with same spin), which is almost, though not entirely, equivalent to the Coulomb hole (correlation between electrons with opposite spin). Thus, there is an error of more than 10%.

2.3 DENSITY FUNCTIONAL THEORY

The HF method formally scales as N^4, where N is the number of basis functions. Thus, the HF method cannot be applied to very big systems. In addition, the method lacks Coulomb-hole correlation

The density functional theory (DFT) is based on electron density instead of a orbital (one-electron wave function) like in HF. The density functional theory, principle is based on the Hohenberg-Kohn theorem and the Kohn-Sham equation.[48] The accuracy and success of DFT depend on the availability of accurate approximations to the exchange-correlation functional. [49-50]

Hohenberg-Kohn demonstrates that the electron density (ρ) determines all ground state properties of a system, which is the function of position: $\rho = \rho$ (x, y, z). The energy of DFT can be written in its simplest form as

$$E_{DFT} = T[\rho] + V_{ext}[\rho] + V_{ee}[\rho] \tag{2.12}$$

or in the line of kohn-sham equation

$$E_{DFT} = T_s[\rho] + V_{ext}[\rho] + J[\rho] + E_{xc}[\rho] \tag{2.13}$$

Which $$J[\rho] = \frac{1}{2}\iint \frac{\rho(r_1)\rho(r_2)}{|\vec{r}_1 - \vec{r}_2|} d\vec{r}_1 d\vec{r}_2$$

$$E_{xc}(\rho) = E_x(\rho) + E_c(\rho) = T[\rho] - T_s[\rho] + V_{ee}[\rho] - J[\rho]$$

where $T[\rho]$ is the kinetic, $T_s[\rho]$ is kinetic of non-interacting system, $V_{ee}[\rho]$ is electron-electron repulsion, $J[\rho]$ is the Columbic interaction, $V_{ext}[\rho]$ is external potential, $E_{xc}(\rho)$ is exchange-correlation functional, $E_x(\rho)$ is exchange functional, and $E_c(\rho)$ is correlation functional.

Hohenberg-Kohn's second theorem proves that E_{DFT} can be obtained from trial density via the variational principle.

Kohn and Sham suggested that the trial density can be obtained from Kohn-Sham orbital, φ_i .

Thus, $$\rho(\vec{r}) = \sum_i |\varphi_i(\vec{r})|^2 \tag{2.14}$$

The Kohn-Sham orbital could be determined from the Kohn-Sham equation

$$\left[-\frac{\nabla^2}{2} + V_s(r)\right]\varphi_i(r) = \varepsilon_i \varphi_i(r) \tag{2.15}$$

where $V_s(r)$ = Kohn-Sham potential

$$= V_{ext}[\rho] + \frac{\delta J[\rho]}{\delta\rho(r)} + \frac{\delta Exc[\rho]}{\delta\rho(r)} \tag{2.16}$$

$$= \sum_{A} \frac{Z_A}{|R_A - r_i|} + \int \frac{\rho(r)}{|r - r^{/}|} dr^{/} + \frac{\delta Exc[\rho]}{\delta\rho(r)} \tag{2.17}$$

and ε_i = Kohn-Sham orbital energy.

Exchange-correlation functional

The art of developing approximations for the exchange–correlation in DFT calculations can be classified into four generations.

1. Local-density approximations (LDA). Exc assumes that at each point in real space, the exchange -correlation energy at that point depend on electron density ρ(r) and obtained of the homogeneous electron gas.
   Examples: (exchange) X-alpha, (correlation) VWN, (xc) SVWN.
2. Generalized gradient approximation (GGA) gave improvement over the LDA. Exc [ρ] involve both the electron density ρ(r) and gradient of the charge density Δρ.
   Examples: (exchange) B86, PW91, (correlation) LYP, PBE. (xc) BLYP, PW91.
3. Meta-GGA (MGGA) is constructed using the second derivative of the electron density ρ(r) and gradient of the charge density Δρ.
   Example: TPSS, Minnesota functional (M05, M06).
4. Hybrid functional is a final class of approximations to the exchange–correlation energy, which mix the exchange and correlation (XC) energy component of the total energy of a system of electrons and meta-GGA,GGA exchange functionals.
   Example: (hybrid) B3LYP, BHRHLYP, B3P86, PBE0.

จุฬาลงกรณ์มหาวิทยาลัย
CHULALONGKORN UNIVERSITY

2.4 BASIS SET

A basis set in theoretical and computational chemistry is a set of functions with known analytical from Fock equation. Thus, the mathematical representations of molecular orbitals are needed to begin such quantum mechanical calculations. Thus, the choice of basis set can be used in quantum chemical calculations.

There are two types of basis functions, Slater type orbitals (STO)[51] and Gaussian type orbitals (GTO) [52].

2.4.1 Slater type atomic orbitals

The slater-type orbitals (STO) is a natural basis set for expansion of the atomic and molecular wavefunctions to solve the Schrödinger equation of H atom. Thus,

$$\phi^{STO}(r,\theta,\phi) = R_n^{STO}(r)Y_{lm}(\theta,\phi) \tag{2.17}$$

where R_{nl}^{STO} = radial part of wavefunction

$$= \frac{(2\xi)^{\frac{3}{3}}}{\sqrt{(2l+2)}}(2\xi)^{l1}e^{-\xi r} \tag{2.18}$$

and $Y_{lm}(\theta,\phi)$ = spherical harmonic function.

The STO is introduced as a simple analytical form of atomic orbitals with standard values recommended by Slater. The limitation of STO is the complicated nature of many-center STO matrix elements arising from the electron-electron interaction. One of the bottleneck issues is the cost of the two-electron integral calculation due to its large number.

2.4.2 Gaussian type atomic orbitals

The Gaussian Type Orbitals (GTO) can be written as

$$\phi = Nx^a y^b z^c e^{-\alpha r 2} \tag{2.19}$$

where x, y, and z are Cartesian coordinates and a, b and c are non-negative integers. GTO's have one enormous advantage, a new algorithmic method developed to evaluate two-electron repulsion integrals can be evaluated without resourcing to numerical integration.

2.4.3 Types of basis sets

2.4.3.1 Minimal basis sets

The minimum basic set is one that includes each atom in the molecule. A single basic function to use for each orbital in the Hartree-Fock calculations on free atoms. The most general minimal basis set is STO-nG, where n represents the number of the number of Gaussian primitive functions used to represent each Slater-type orbital. Based on these foundational sets the same number of Gaussian primitives comprises the core and valence orbitals. Minimal basis sets give rough results that are insufficient to publish research quality but are cheaper than a pair of them. Commonly used minimal basis sets of this generic type are: STO-3G, STO-4G, etc.

จุฬาลงกรณ์มหาวิทยาลัย
Chulalongkorn University

2.4.3.2 Extended basis sets

The minimal basis sets are not flexible enough for accurate representation of orbitals. It requires the use of multiple functions to represent each atomic orbital.

Split-Valence

Split-Valence basis sets as the description of valence orbitals is split into two (or more) basis functions. developed to overcome problems of inadequate description of anisotropic electron distributions in molecules using minimal basis sets. The most common split-valence is X-YZ G, where X represents the number of primitive Gaussians comprising each core atomic orbital basis function, Y and Z represent the valence orbitals, which are composed of two basis functions each, the first one

composed of a linear combination of Y primitive Gaussian functions, the other composed of a linear combination of Z primitive Gaussian functions. For example, 6-31G is a split valence basis set in which six primitive Gaussians comprise each core atomic orbital basis function and two basis functions for each AO (double-zeta).

Polarized basis sets

Polarized basis sets add orbitals, indicating the level of angular. The momentum functions included go beyond those necessary for an appropriate description of the ground state of each atom. For example, the basis function located on a hydrogen atom in a minimal basis set would be a function approximating the 1s atomic orbital. Thus, polarized basis sets add p-functions of hydrogen atoms. Polarization accounts for these influences, which distort the orbital shape. For both polarized basis sets, 6-31G** and 6-31G (d, p) are similar where p-type functions are added to H atoms, d-type functions are added to atoms with Z > 2 and f-type functions are added to transition metals.

จุฬาลงกรณ์มหาวิทยาลัย
CHULALONGKORN UNIVERSITY

CHAPTER III
DETAILS OF THE CALCULATION

3.1 COMPUTATIONAL METHOD

All DFT calculations are implemented in the Gaussian 09 suite of programs.[53] For the exchange-correlation functional, Minnesota's hybrid meta generalized gradient approximation (mGGA) M06-2X was used. A double-zeta basis set (DZ) with d-type Cartesian-Gaussian polarization functions for heavy atom, was employed using the 6-31g (d) basis sets. The convergence criteria for the geometry optimization and energy calculation were converged to within 10^{-6} Hartree. The computed HOMO-LUMO gap energy is defined using

$$\text{HOMO-LUMO gap} = E_{LUMO} - E_{HOMO} \tag{3.1}$$

where E_{LUMO} and E_{HOMO} are energies of the lowest unoccupied molecular orbital (LUMO) and the highest occupied molecular orbital (HOMO), respectively.

The Hydrogen adsorption energy (E_{ad}) of H_2 and GQDs was calculated by

$$E_{ad} = E_{GQD+\,H2} - E_{GQDs} - E_{H2} \tag{3.2}$$

จุฬาลงกรณ์มหาวิทยาลัย
CHULALONGKORN UNIVERSITY

where E_{ad} is adsorption energy, E_{GQDs} is total energy of pristine GQDs, E_{H2} is total energy of the H_2 molecule, E_{GQD+H2} is total energy of the adsorption complex. According to this definition, a negative value of E_{ad} denotes a favorable adsorption process.

3.2 GEOMETRIES OF GQDS

The effects of external electric fields (EEFSs), from-0.035 to +0.035 a.u., on the geometries and electronic properties of graphene quantum dots (GQDs), i.e., $C_{24}H_{12}$, $C_{54}H_{18}$, and $C_{96}H_{24}$, were investigated as displayed in **Figure 2**. According to the symmetry analysis shown in **Figure 3**, three sizes of GQD structures, (a) $C_{24}H_{12}$, (b)

$C_{54}H_{18}$, and (c) $C_{96}H_{24}$, can be curved in two directions, namely along the C atom and along the C-C bond.

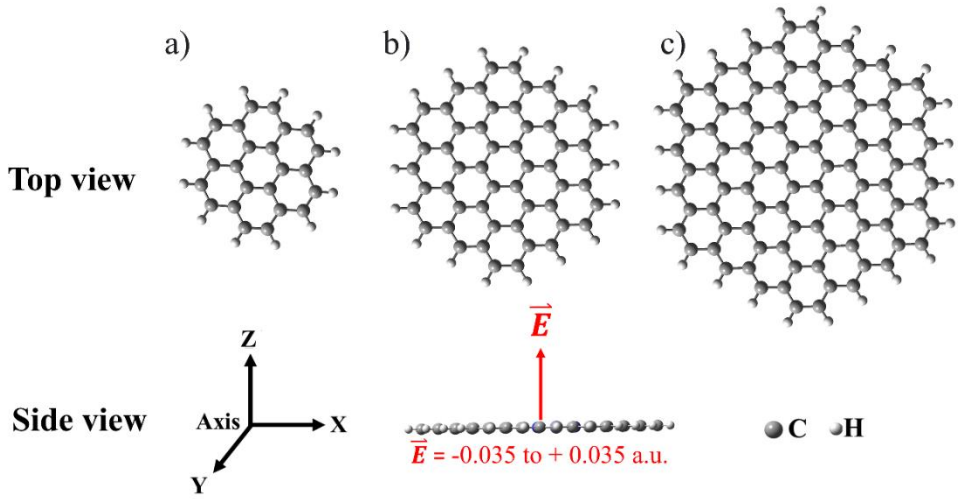

Figure 2 The geometry of (a) $C_{24}H_{12}$, (b) $C_{54}H_{18}$, and (c) $C_{96}H_{24}$ and the direction of the applied field.

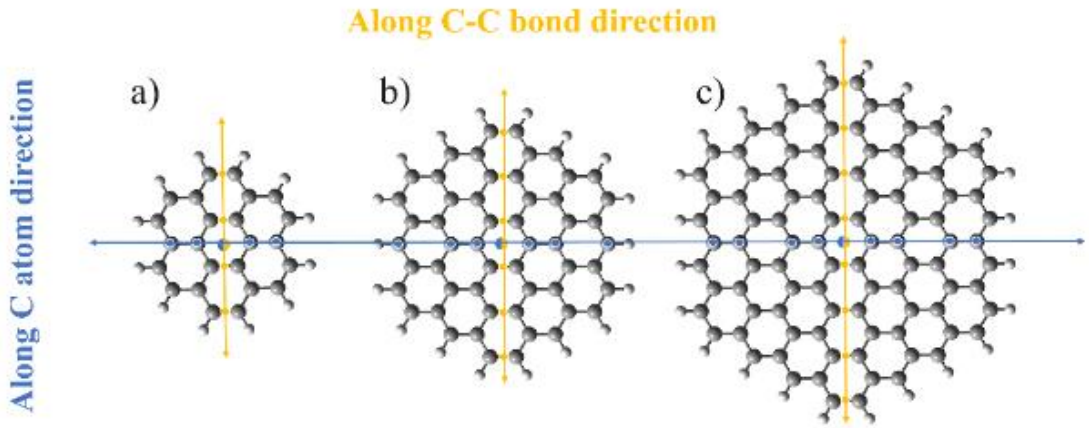

Figure 3 Two curving directions, along C atoms and C-C bond directions, of (a) $C_{24}H_{12}$, (b) $C_{54}H_{18}$, and (c) $C_{96}H_{24}$.

3.3 GEOMETRIES OF m-4N-GDQs

The functionalized m-4N-GDQs structures contain 96 carbon atoms, of which two carbon atoms were removed, followed by the substitution of the four carbon atoms around the divacancy defect with four nitrogen atoms to provide the anchoring site

for various metal atom ions (Ca, Ca^{2+}, Cr, Cr^{2+}, Fe, and Fe^{2+}). The external electric field, from -0.035 to +0.035 a.u., was applied to the structures. **Figure 4**. The curving directions, i.e., along C atoms and C-C bond directions, of m-4N-GQDs were defined. Eight points for the C-C bond direction and seven points for the C atom direction were observed (**Figure 5**). In contrast to GQDs, the m-4N-GQDs generate asymmetric folding.

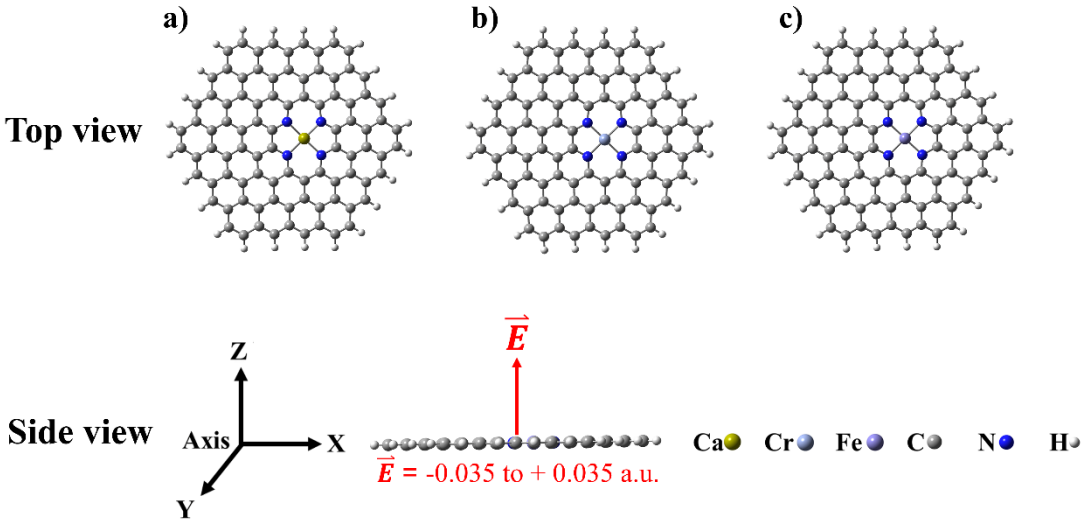

Figure 4 Schematic of the metal-4N-GDQs models (metal; Ca, Ca^{2+}, Cr, Cr^{2+}, Fe, and Fe^{2+})

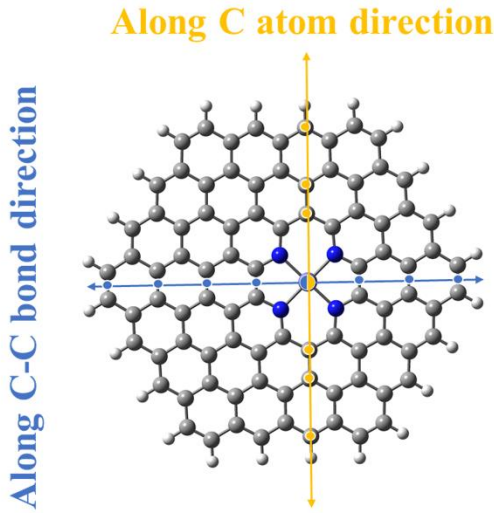

Figure 5 Two curving directions, along C atoms and C-C bond directions, m-4N-GQDs.

3.4 H_2-ADSORPTION ON CURVED Fe^{2+}-4N-GDQS

Single point calculations were performed on several curved Fe2+-4N-GDQS, in which their geometries were optimized from 3.2. H_2 was placed in an on-top position at various distances between Fe^{2+} and the H_2 center, from 2.5 Å to 4.0 Å as displayed in **Figure 6**.

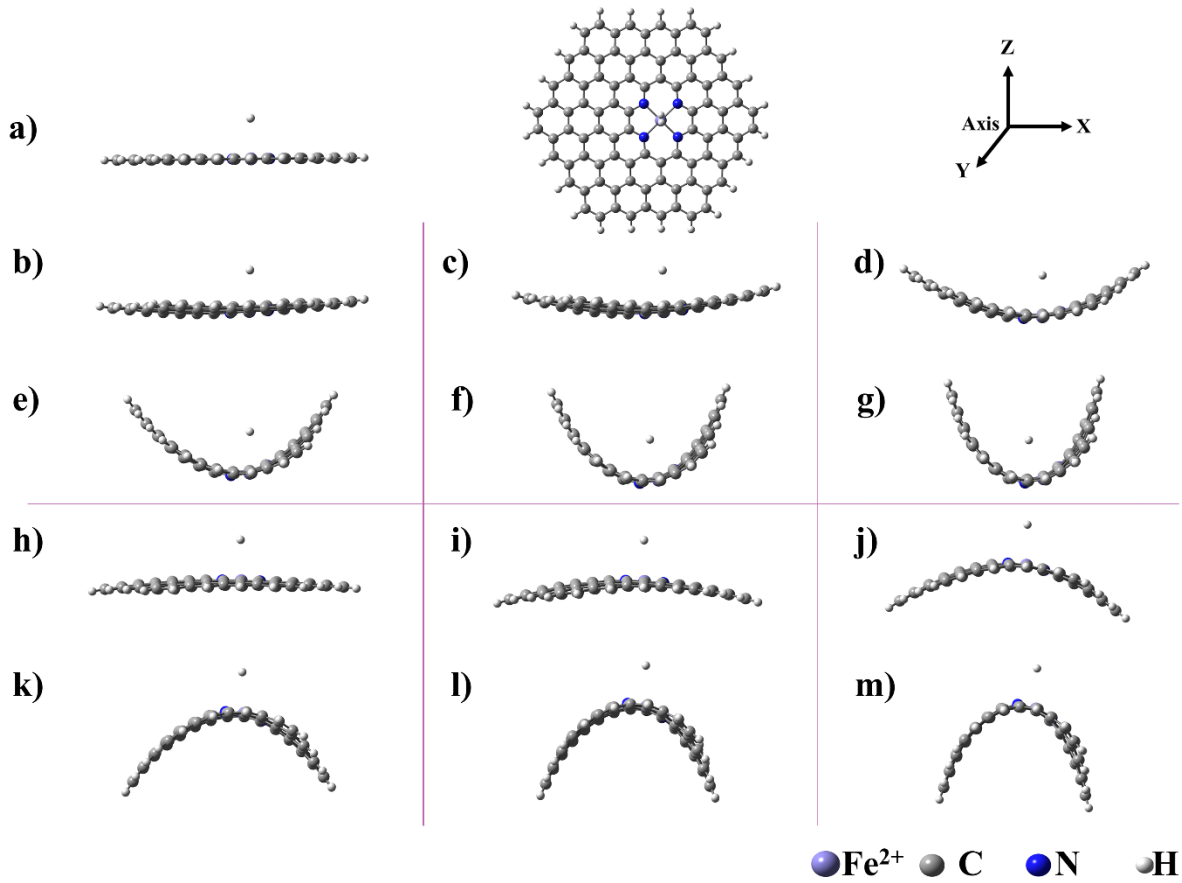

Figure 6 The adsorption of H_2 on curved Fe^{2+}-4N-GDQs with various degrees of curvature, a) = 0, b) = -0.00728 c) = -0.01694, d) = -0.04018 e) = -0.06512, f) = -0.08139, g) = -0.0915, e) = 0.00728, f) = 0.01694, g) = -0.04018., k) = 0.06512, l) = 0.08139, m) = 0.0915.

CHAPTER IV
RESULTS AND DISCUSSION

4.1 THE EFFECT OF EXTERNAL ELECTRIC FIELD ON MOLECULAR STRUCTURE

4.1.1 CURVING OF GQDs BY EEFSs

GDQs, i.e., $C_{24}H_{12}$, $C_{54}H_{18}$, and $C_{96}H_{24}$ are curved when applying external electric fields (EEFSs). GDQs is curved along the direction of the external electric field (Z-axis), which is based on electric field strength. The curves of GDQs under negative and positive electric fields are the opposite directions, as displayed in **Figure 7**. The curves of three sizes of GQD structures, $C_{24}H_{12}$, $C_{54}H_{18}$, and $C_{96}H_{24}$, in two directions, namely along the C atom and the C-C bond, were defined. The curvature of $C_{24}H_{12}$, $C_{54}H_{18}$, and $C_{96}H_{24}$ was plotted between Z coordinate variation (ΔZ) and distance from the center. The curved GQDs in two directions were shown in **Appendix Figures A1, A3, and A5** for the C atom direction and **Appendix Figures A2, A4, and A6** for the C-C bond direction. **From Appendix Figure A1-6**, the results show that the $C_{54}H_{18}$ and $C_{96}H_{24}$ preferred curved over C atom directions, while the $C_{24}H_{12}$ slightly preferred curved over the C-C bond direction. The curvature of GQDs tends to have more curves as the size of the GQDs increases.

จุฬาลงกรณ์มหาวิทยาลัย
CHULALONGKORN UNIVERSITY

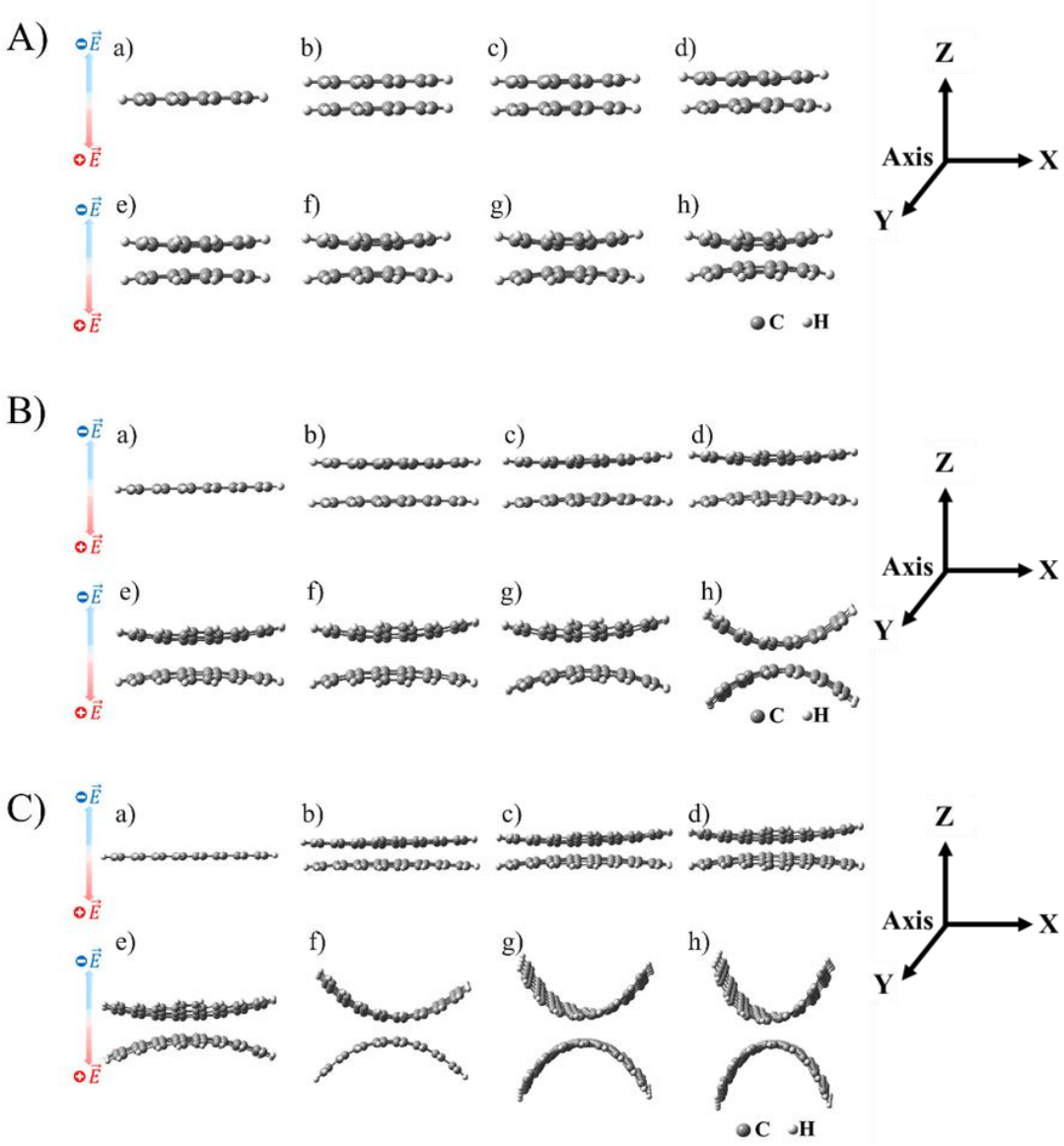

Figure 7 Geometries optimization of GDQs model, of (A) $C_{24}H_{12}$, (B) $C_{54}H_{18}$, and (C) $C_{96}H_{24}$, with different electric fields, a) = 0.0 a.u., b) = 0.010 a.u., c) = 0.0150 a.u., d) = 0.020 a.u., e) = 0.025 a.u., f) = 0.030 a.u. g) = 0.035 a.u.

The curved shapes of $C_{24}H_{12}$, $C_{54}H_{18}$, and $C_{96}H_{24}$ are shown in **Appendix Figures A2, A3, and A5**, respectively. The plots have a parabolic shape. Thus, we fit their graph using the quadratic equation ($\Delta Y = aX^2 + bX + c$), x being the distance from the center, which shows a good fit with an R^2 of above 0.097. The coefficient "a" represents the degree of curvature where at EEFSs = 0.000 a.u., a is "0," which implies the structure is planar. When the EEFSs is positive, the function is convex, while when it is negative, it is concave downward. **Figure 8** shows how the degree of curvature or absolute value |a| varies with the external electric field for $C_{24}H_{12}$, $C_{54}H_{18}$, and $C_{96}H_{24}$. The results indicated that the curvature of GQDs increased with increasing electric field strength. Both the curvature of GQDs under the negative and positive electric field are equivalent, but they curve in the opposite direction. The degree of curvature of $C_{96}H_{24}$ is higher than $C_{54}H_{18}$ and $C_{24}H_{12}$, respectively. As the calculated dipole moments of $C_{24}H_{12}$, $C_{54}H_{18}$, and $C_{96}H_{24}$ increase under external electric fields ranging from -0.035 to +0.035 a.u., so does the degree of curvature, which is why it is preferable to curve the same direction with an external EFFs (Z axis). An external electric field can induce dipole moments. The curved structure is stabilized by EEFSs owing to the dipole moment.

However, the dipole moments of EFFs with positive and negative charge are opposite on the Z-axis, which causes the curvature of GQDs to be curved in the opposite direction also. The results show that the curving of $C_{24}H_{12}$, $C_{54}H_{18}$, and $C_{96}H_{24}$ are based on the value and direction of the dipole moments. The field-dependent energy is giving by

$$E(F)=E_0 - \mu F + 1/2\alpha F^2 + ...$$

Therefore, the structure with a positive dipole moment will be stabilized by a positive electric field and vice versa.

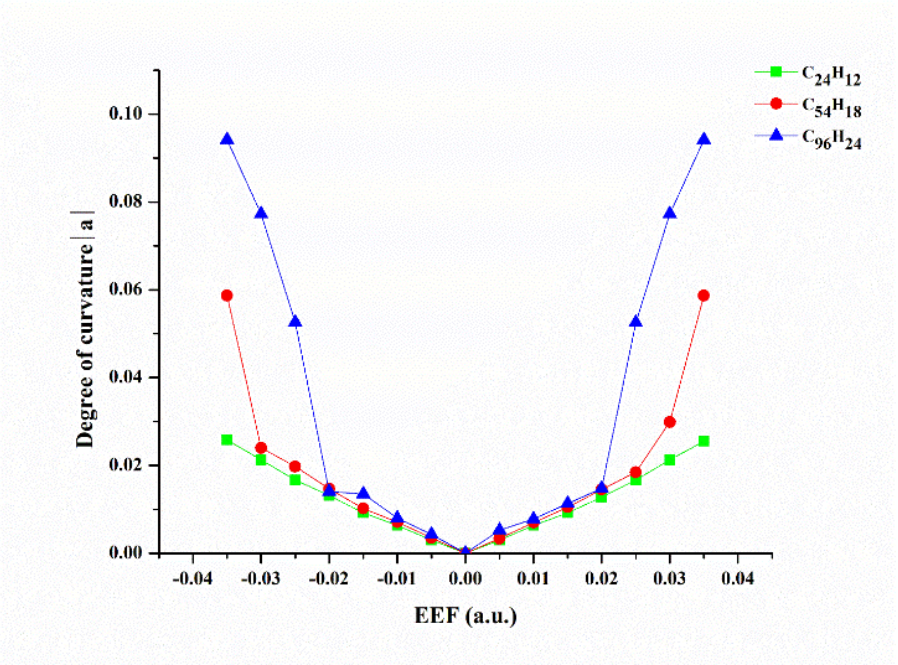

Figure 8 Dependent of the degree of curvature on external electric field for $C_{24}H_{12}$, $C_{54}H_{18}$, and $C_{96}H_{24}$.

จุฬาลงกรณ์มหาวิทยาลัย
CHULALONGKORN UNIVERSITY

Table 1 Dipole moment of $C_{24}H_{12}$, $C_{54}H_{18}$, and $C_{96}H_{24}$ under external electric fields from -0.035 to +0.035 a.u.

	Dipolement (Debye)											
EEFS	$C_{24}H_{12}$				$C_{54}H_{18}$				$C_{96}H_{24}$			
(a.u.)	x	y	z	Total	x	y	z	Total	x	y	z	Total
0.035	0	0	-8.18	8.18	-0.01	0.03	-26.49	26.49	0	0	-67.74	67.74
0.03	0	0	-6.89	6.89	0	0.01	-18.9	18.9	0	0	-49.19	49.19
0.025	0	0	-5.65	5.65	0	0	-15.17	15.17	0.01	0.03	-30.82	30.82
0.02	0	0	-4.46	4.46	0	0	-11.95	11.95	0	0	-17.13	17.13
0.015	0	0	-3.31	3.31	0	0	-8.81	8.81	0	0	-12.45	12.45
0.01	0	0	-2.2	2.2	0	0	-5.87	5.87	0	0	-8.1	8.1
0.005	0	0	-1.1	1.1	0	0	-2.9	2.9	0	0	-4.08	4.08
0	0	0	0	0	0	0	0	0	0	0	0	0
-0.01	0	0	2.2	2.2	0	0	5.88	5.88	0	0	8.12	8.12
-0.015	0	0	3.31	3.31	0	0	8.84	8.84	0	0	12.42	12.42
-0.02	0	0	4.46	4.46	0	0	11.93	11.93	0	0	17.04	17.04
-0.025	0	0	5.65	5.65	0	0	15.19	15.19	-0.01	-0.02	30.82	30.82
-0.03	0	0	6.89	6.89	0	0	18.47	18.47	0	0	49.2	49.2
-0.035	0	0	8.18	8.18	0.01	0.03	26.49	26.49	0	0	67.73	67.73

จุฬาลงกรณ์มหาวิทยาลัย
Chulalongkorn University

4.1.2 CURVING OF m-4N-GQDs BY EEFSs

The m-4N-GDQs with various metal substituents were investigated in different external electric fields. **Figures 9 and 10** show the geometries optimization of m-4N-GDQs with different external electric fields for neutral metal ions (Ca, Cr, and Fe) and metal (II) ions (Ca^{2+}, Cr^{2+}, and Fe^{2+}). The m-4N-GDQs have a convex structure with the electric field of a positive charge, while they have a concave structure with the electric field of a negative charge. The curvature of m-4N-GDQs is increased, which increases the electric field. The curved m-4N-GDQs is directly related to the strength of the electric field. The Ca and Ca^{2+} substituents are moved away from the metal-4N-GDQs plane because the Ca and Ca^{2+} atoms are bigger than other metal atoms. The distance from the 4N center and ΔY coordinate in the C-C bond direction of Ca, Ca^{2+}, Cr, Cr^{2+}, Fe, and Fe^{2+} were plotted in **Appendix Figures A7, A9, A11, A13, A15, and A17**, respectively. On the other hand, the distance from the 4N center and ΔY coordinate in the c atom direction of Ca, Ca^{2+}, Cr, Cr^{2+}, Fe, and Fe^{2+} were plotted in **Appendix Figures A8, A10, A12, A14, A16, and A18**, respectively. The m-4N-GQD curvatures are specified in the C-C bond direction. With increasing EEFS, the curvature of the m-4N-GQDs increases. The m-4N-GQDs curvature depends on the strength of the electric field.

จุฬาลงกรณ์มหาวิทยาลัย
CHULALONGKORN UNIVERSITY

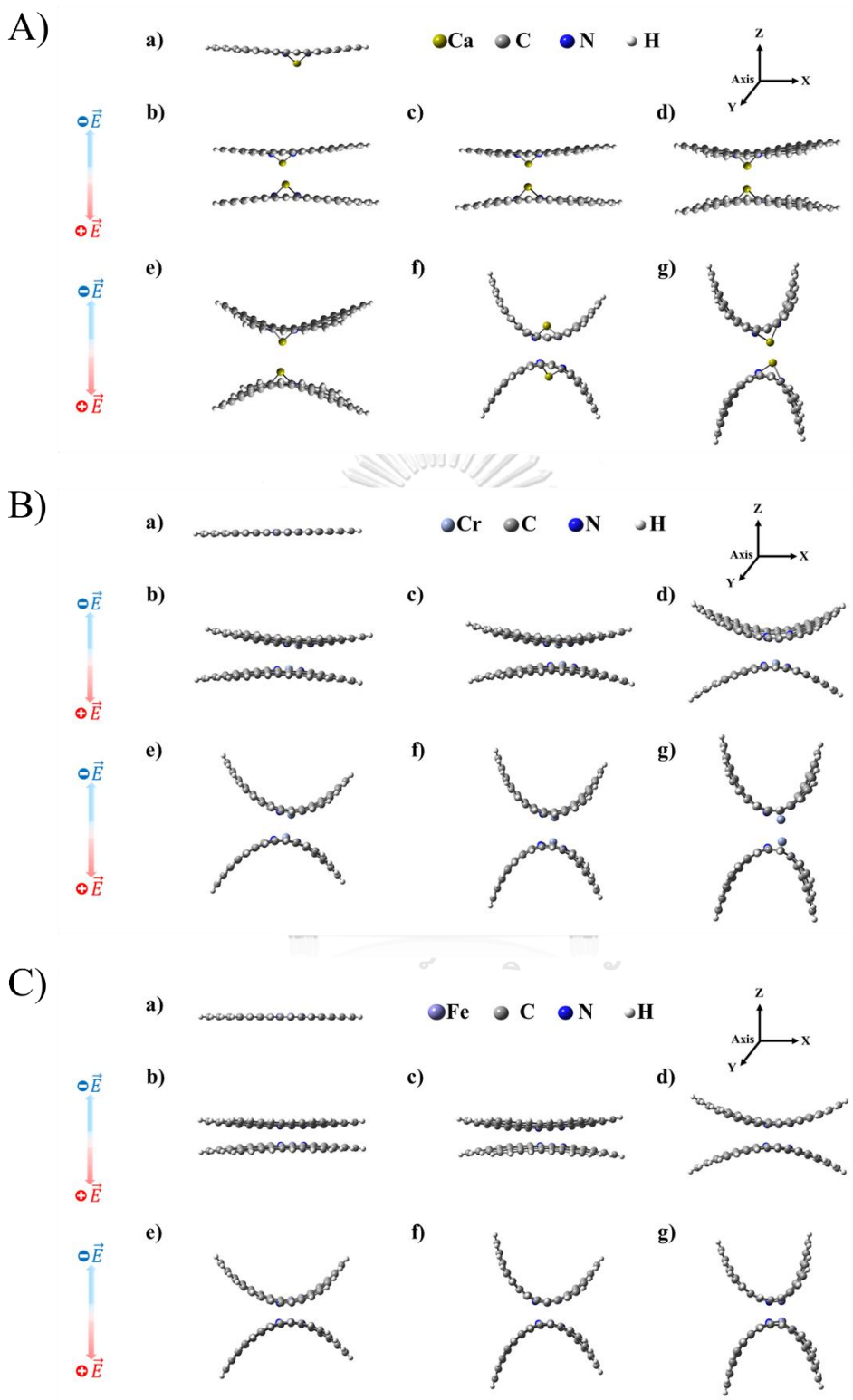

Figure 9 Geometries optimization of m-4N-GDQs model, of (A) Ca, (B) Cr, and (C) Fe, with different electric fields, a) = 0.0 a.u., b) = 0.010 a.u., c) = 0.0150 a.u., d) = 0.020 a.u., e) = 0.025 a.u., f) = 0.030 a.u. g) = 0.035 a.u.

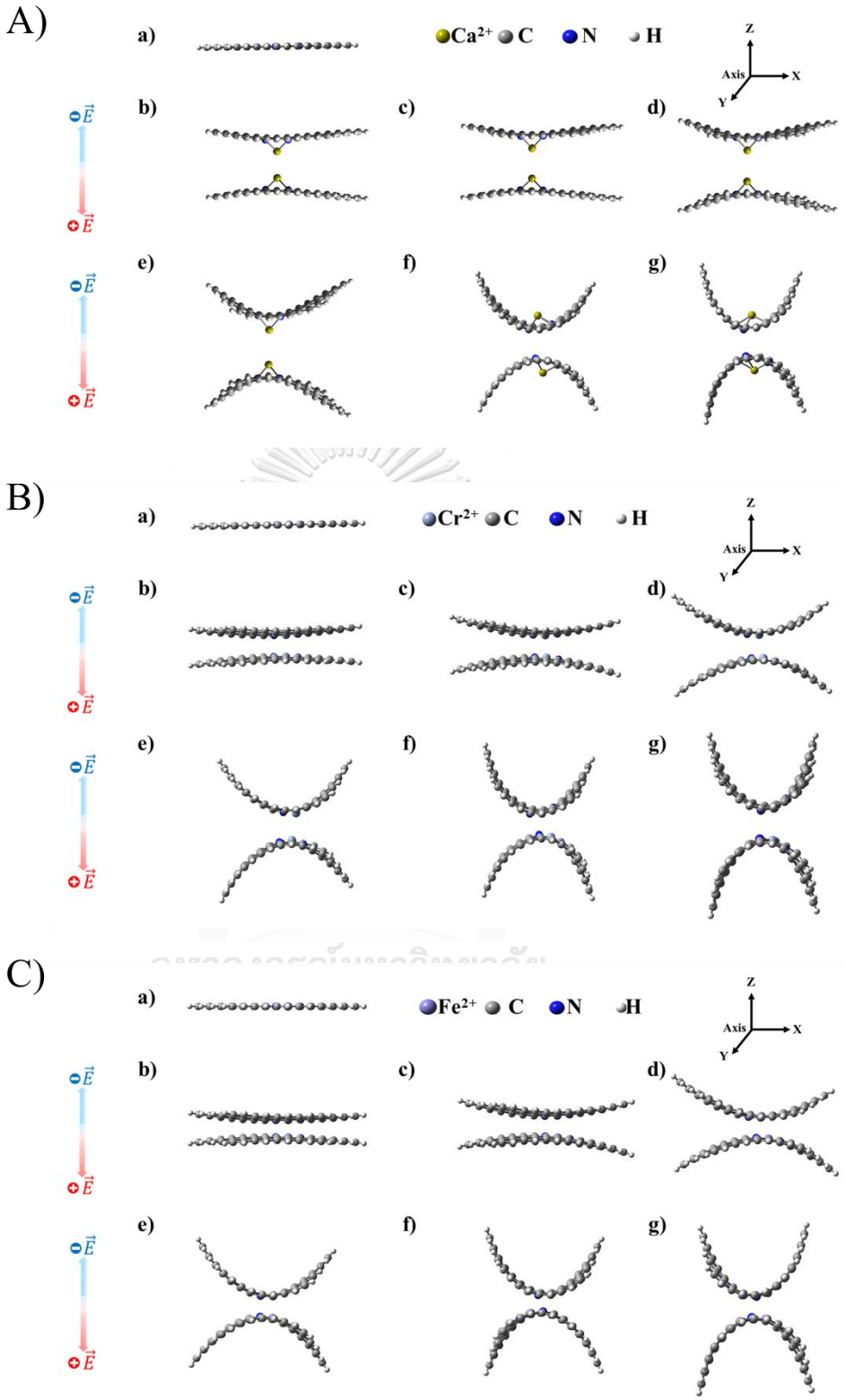

Figure 10 Geometries optimization of m-4N-GDQs model, of (A) Ca^{2+}, (B) Cr^{2+}, and (C) Fe^{2+}, with different electric fields, a) = 0.0 a.u., b) = 0.010 a.u., c) = 0.0150 a.u., d) = 0.020 a.u., e) = 0.025 a.u., f) = 0.030 a.u. g) = 0.035 a.u.

It is well known that the curved m-4N-GQD is specific in the C-C bond direction. From **Appendix Figures A17, A19, A21, A23, A25, and A27**, the curve between the distance from the 4N center and the ΔY coordinate in the C-C bond direction can be fitted by a quadratic equation similar to the case of GQDs.

Thus, the curvature of the curved m-4N-GQDs can be estimated. We make the absolute coefficient variables of the second derivative, called the degree of curvature, and the external electric fields of m-4N-GQDs, $R^2 > 0.097$, as displayed in **Figure 11**. The Ca and Ca^{2+} of 4N-GDQs can be fitted by a quadratic equation at 0.025-0.035 a.u., which another metal has a similar trend. The m-4N-GQD curvature is mirrored in an electric field with negative and positive polarity.

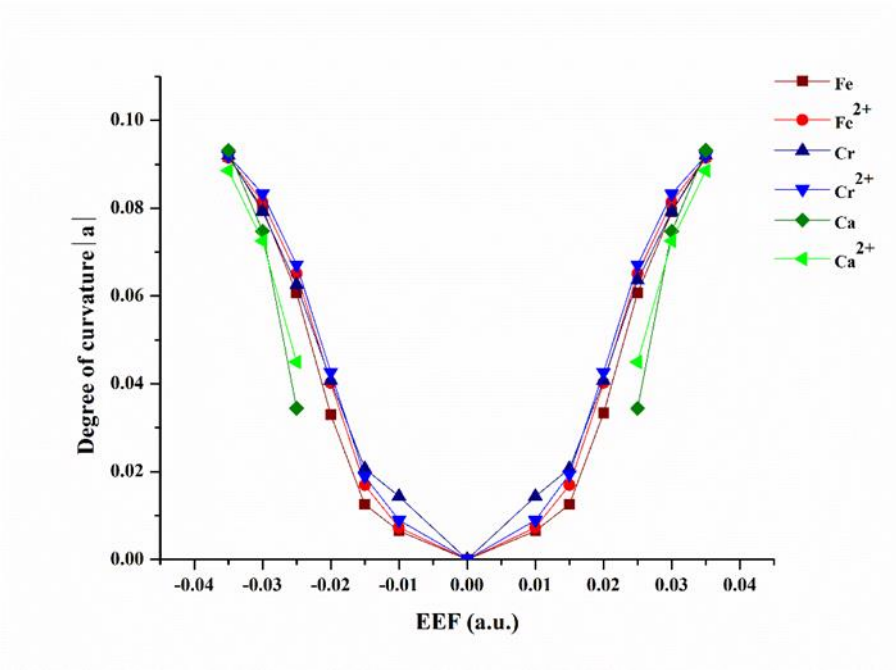

Figure 11 Dependent of the degree of curvature on external electric field for m-4N-GDQs.

The dipole moment of m-4N-GDQs, i.e., Ca, Cr, Fe, Ca^{2+}, Cr^{2+}, Fe^{2+}, under external electric fields from-0.035 to +0.035 a.u were investigated and shown in **Table 2** and **Table 3**, respectively. With increasing EEFS, the dipole moment of m-4N-GDQs is along the EEFS direction (Z-axis). The dipole moment of m-4N-GDQs increases rapidly with the increase in EEFS. In the Z-axis between EEFS with negative and positive

charge, the dipole moment of m-4N-GDQs is opposite. Except in the highest electric field, the dipole moment of m-4N-GDQs is lower than that of m(II)-4N-GDQs. In the same metal doping, the dipole moment of m-4N-GDQs is higher than that of m(II)-4N-GDQs. The dipole moment of m-4N-GDQs decreases as the number of electrons increases (Ca > Cr > Fe), whereas m(II)-4N-GDQs shows no trend. The dipole moment of m-4N-GDQs and m(II)-4N-GDQs follows similar patterns. The dipole moment of m-4N-GDQs is Ca > Cr > Fe, whereas the dipole moment of m(II)-4N-GDQs is Ca^{2+} > Fe^{2+} > Cr^{2+}. When the dipole moment is small, m-4N-GDQs and m(II)-4N-GDQs have small deformations. The findings show that the curving of m-4N-GDQs and m(II)-4N-GDQs is affected by the value and direction of the dipole moments. However, the dipole moment of GQDs and m-4N-GDQs are zero and non-zero, respectively, when an applied electric field affects m-4N-GDQs higher than GQDs, which causes the degree of curvature of m-4N-GDQs to be higher than GDQs.

จุฬาลงกรณ์มหาวิทยาลัย
CHULALONGKORN UNIVERSITY

Table 2 Dipole moment of Ca, Cr and Fe-4N-GDQs under external electric fields from -0.035 to +0.035 a.u.

EEFSs	Dipolement (Debye)											
	Ca				Cr				Fe			
(a.u.)	x	y	z	Total	x	y	z	Total	x	y	z	Total
0.035	0.00	4.86	-118.69	118.79	0.00	-3.37	-107.15	107.20	0.00	-1.87	-90.12	90.14
0.030	0.00	4.54	-58.45	58.62	0.00	-3.47	-62.45	62.55	0.00	-2.85	-59.40	59.47
0.025	0.00	1.88	-31.68	31.73	0.00	2.64	-38.78	38.87	0.00	-2.61	-38.04	38.13
0.020	-2.03	0.00	-22.99	23.08	0.00	-2.12	-22.88	22.98	-0.32	-2.19	-20.61	20.73
0.015	1.85	0.00	-18.23	18.32	-1.96	0.00	-13.53	13.68	-2.14	0.00	-12.87	13.05
0.010	-1.69	0.00	-14.01	14.11	-1.94	0.00	-8.78	8.99	-2.14	0.00	-8.25	8.52
0.000	-1.69	0.00	-14.01	14.11	-2.00	0.00	0.00	2.00	-2.13	0.00	0.00	2.13
-0.010	-1.69	0.00	14.01	14.11	-1.94	0.00	8.78	8.99	-2.14	0.00	8.25	8.52
-0.015	-1.85	0.00	18.23	18.32	-1.96	0.00	13.53	13.68	-2.14	0.00	12.87	13.05
-0.020	-2.03	0.00	22.99	23.08	0.00	-2.12	22.88	22.98	0.00	-2.21	20.70	20.82
-0.025	0.00	-1.88	31.68	31.73	0.00	2.64	38.78	38.87	0.00	-2.61	38.04	38.13
-0.030	0.00	4.54	58.45	58.62	0.00	-3.47	62.45	62.55	0.00	-2.85	59.40	59.47
-0.035	0.00	4.86	118.69	118.79	0.00	-3.37	107.15	107.20	0.00	-1.87	90.12	90.14

จุฬาลงกรณ์มหาวิทยาลัย
CHULALONGKORN UNIVERSITY

Table 3 Dipole moment of Ca^{2+}, Cr^{2+}, and Fe^{2+}-4N-GDQs under external electric fields from -0.035 to +0.035 a.u..

EEFS	Dipole moment (Debye)											
	Ca^{2+}				Cr^{2+}				Fe^{2+}			
(a.u.)	x	y	z	Total	x	y	z	Total	x	y	z	Total
0.035	0.00	4.31	-86.84	86.95	0.00	-0.83	-94.34	94.34	0.00	5.37	-87.74	87.90
0.030	0.00	6.19	-62.17	62.48	0.00	-3.99	-71.45	71.57	0.00	6.84	-67.12	67.47
0.025	0.00	-2.94	-34.97	35.10	0.00	7.95	-47.22	47.89	0.00	-8.04	-45.56	46.27
0.020	3.99	0.00	-23.94	24.27	0.00	-7.07	-26.77	27.69	0.00	7.54	-25.45	26.54
0.015	4.90	0.00	-18.50	19.13	5.83	-0.01	-14.59	15.71	6.12	0.00	-14.07	15.34
0.010	5.40	0.00	-14.10	15.10	5.38	0.00	-8.99	10.48	5.73	0.00	-8.68	10.40
0.000	5.17	0.00	0.00	5.17	5.33	0.00	0.00	5.33	5.75	0.00	0.00	5.75
-0.010	5.40	0.00	14.10	15.10	5.38	0.00	8.99	10.48	5.73	0.00	8.68	10.40
-0.015	4.90	0.00	18.50	19.13	5.82	0.00	14.58	15.70	6.12	0.00	14.07	15.34
-0.020	3.99	0.00	23.94	24.27	0.00	-7.07	26.77	27.69	0.00	-7.54	25.45	26.54
-0.025	0.00	2.94	34.97	35.10	0.00	7.95	47.22	47.89	0.00	-8.04	45.56	46.27
-0.030	0.00	6.19	62.17	62.48	0.00	-3.99	71.45	71.57	0.00	-6.84	67.12	67.47
-0.035	0.00	4.31	86.84	86.95	0.00	-0.83	94.34	94.34	0.00	-5.37	87.74	87.90

จุฬาลงกรณ์มหาวิทยาลัย
CHULALONGKORN UNIVERSITY

4.2 THE EFFECT OF EXTERNAL ELECTRIC FIELD ON ELECTRONIC PROPERTY

4.2.1 THE EFFECT OF EEFSs ON HOMO-LUMO GAP OF GQDs

The effects of the external electric field on the electronic properties of GQDs, $C_{24}H_{12}$, $C_{54}H_{18}$, and $C_{96}H_{24}$, were compared. We plotted the different electric fields and the HOMO-LUMO gap energies of $C_{24}H_{12}$, $C_{54}H_{18}$, and $C_{96}H_{24}$ as displayed in **Figure 12**. The HOMO-LUMO gap energies are in the order of $C_{24}H_{12} > C_{54}H_{18} > C_{96}H_{24}$, respectively. Moreover, the HOMO-LUMO gap energies were significantly reduced when the applied EEFSs was higher than 0.03 a.u. and 0.025 a.u. of $C_{54}H_{18}$ and $C_{96}H_{24}$, respectively.

These results were inconsistent with previous studies[54] where the HOMO-LUMO gap energy was reduced when the size of GQDs was increased. The degree of curvature, |a|, fitted by a quadratic equation, and the HOMO-LUMO gap energies of $C_{24}H_{12}$, $C_{54}H_{18}$, and $C_{96}H_{24}$ were displayed in **Figure 13**. As can be seen, the curvature degree |a| is increased to reduce HOMO-LUMO gap energies. Although the results appear consistent with prior research, Pattarapongdilok et al.[18] proposed that the HOMO-LUMO gap of graphene quantum dots (GQDs) is indirectly proportional to the degree of folding. The HOMO-LUMO gap energies of $C_{24}H_{12}$, $C_{54}H_{18}$, and $C_{96}H_{24}$ can be turned into EEFS and the degree of curvature |a|.

จุฬาลงกรณ์มหาวิทยาลัย
CHULALONGKORN UNIVERSITY

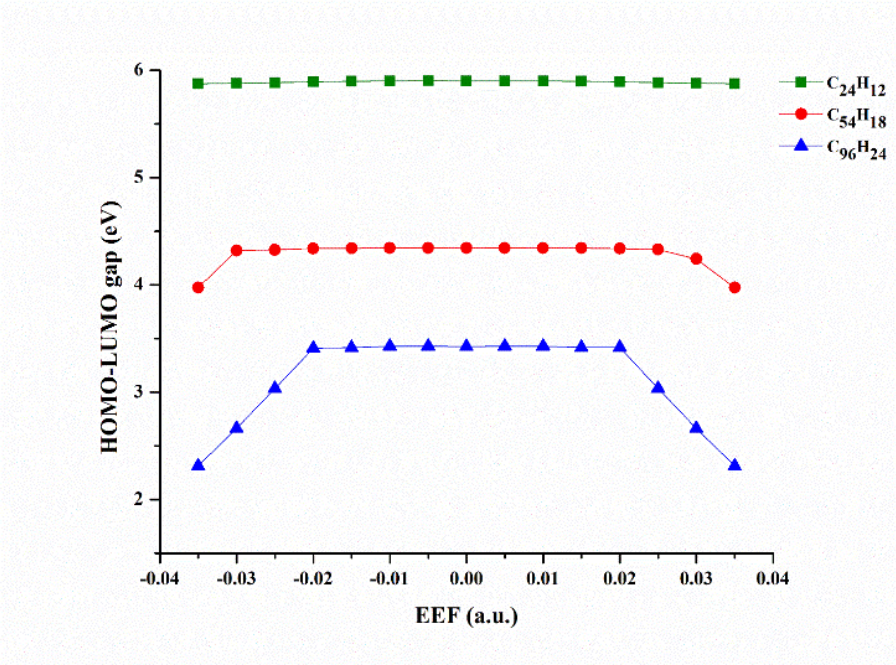

Figure 12 Calculated the different an electric fields and the HOMO-LUMO gap energies of $C_{24}H_{12}$, $C_{54}H_{18}$, and $C_{96}H_{24}$.

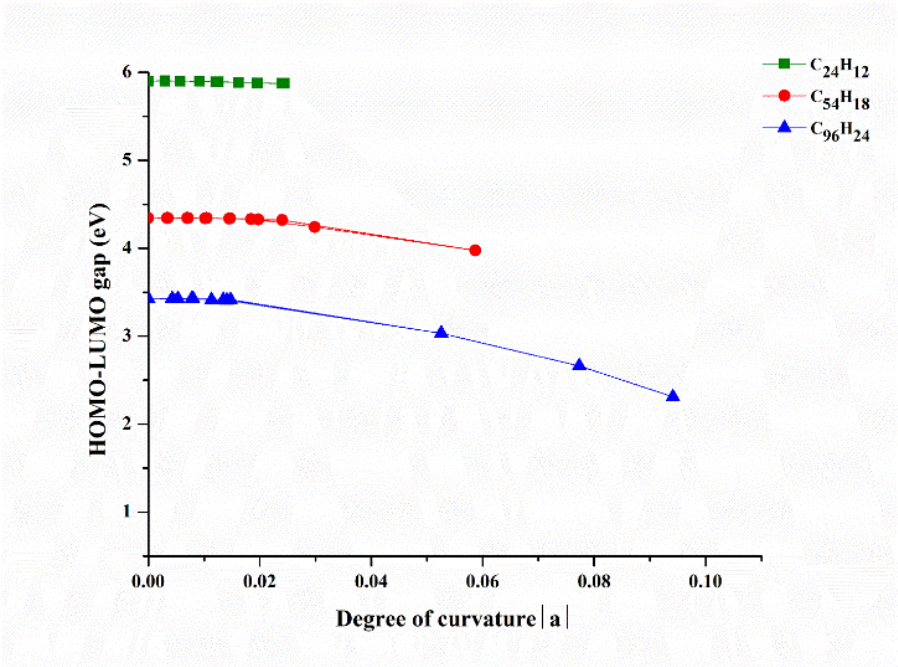

Figure 13 The degree of curvature |a|, fitted by a quadratic equation, and the HOMO-LUMO gap energies of $C_{24}H_{12}$, $C_{54}H_{18}$, and $C_{96}H_{24}$.

4.2.2 THE EFFECT OF EEFSs ON HOMO-LOMO GAP OF 4m-4N-GQDs

We observed the HOMO-LUMO gap of various metals of 4N-GDQs under different external electric fields as displayed in **Figure 14**. With the increase of EEFS higher than 0.02 a.u., the HOMO-LUMO gap of Cr, Cr^{2+}, Fe, and Fe^{2+} showed a significant decrease. For the HOMO-LUMO gap of Ca, it will decrease rapidly when applied EEFS at 0.025 a.u. and 0.035 a.u., while Ca^{2+} will reduce rapidly at 0.030 a.u. and 0.035 a.u. The HOMO-LUMO gap of neutral metal ions (Ca, Cr, and Fe) doped is higher than metal (II) ions (Ca^{2+}, Cr^{2+}, and Fe^{2+}). Moreover, the HOMO-LUMO gap of metal (II) ions is inverted with the electronic structure, which decreases when there is an increasing number of electrons ($Ca^{2+} > Cr^{2+} > Fe^{2+}$). The HOMO-LUMO gap of neutral metal ions doesn't depend on the number of electrons. Moreover, it was found that the HOMO-LUMO gap of m-4N-GDQs can be turned with an external electric field. The degree of curvature, |a|, fitted by a quadratic equation, and the HOMO-LUMO gap energies of m-4N-GDQs were plotted in **Figure 15**. The degree of curvature |a| of Fe-4N-GDQs is related to the HOMO-LUMO gap energies in an indirect manner, similar to Cr, Cr^{2+}, and Fe^{2+}-4N-GDQs except at the final point where the HOMO-LUMO gap energies increase. It is well known that the m-4N-GDQs deformation is related to the HOMO-LUMO gap.

จุฬาลงกรณ์มหาวิทยาลัย
CHULALONGKORN UNIVERSITY

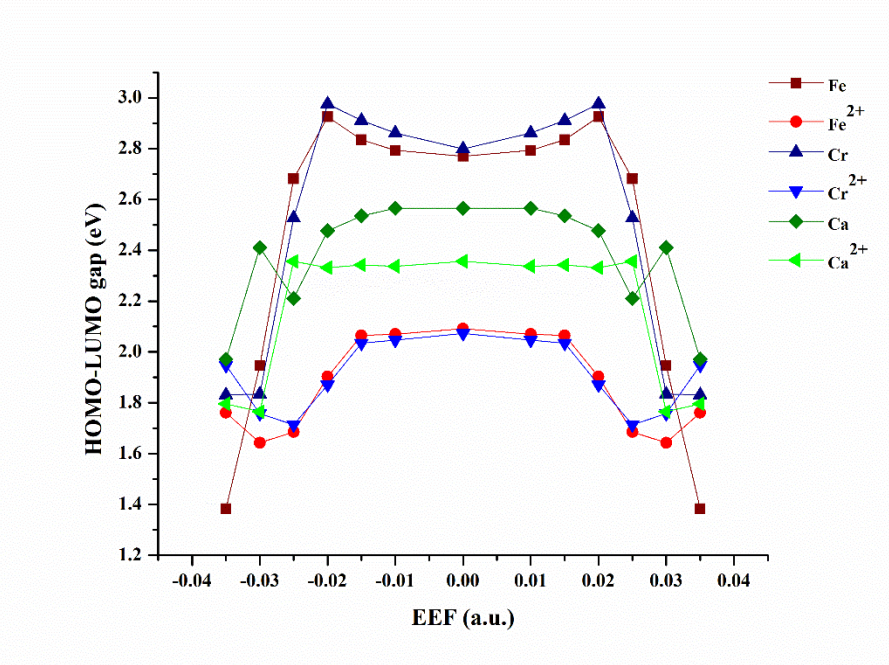

Figure 14 Calculated the different an electric fields and the HOMO-LUMO gap energies of m-4N-GDQs.

จุฬาลงกรณ์มหาวิทยาลัย
CHULALONGKORN UNIVERSITY

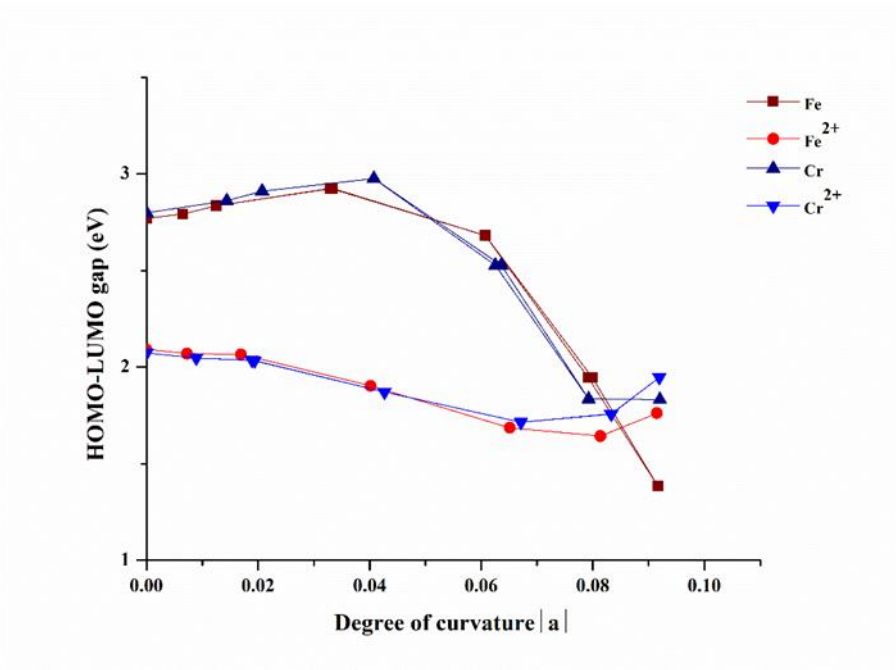

Figure 15 The degrees of curvatures |a|, fitted by a quadratic equation, and the HOMO-LUMO gap energies of m-4N-GDQs.

จุฬาลงกรณ์มหาวิทยาลัย
CHULALONGKORN UNIVERSITY

4.3 THE ADSORPTION OF MOLECULAR H_2 ON CURVED Fe^{2+}-4N-GQDs

The optimized geometry of Fe^{2+}-4N-GDQs with different EEFSs from the previous section was used for the adsorption study, which uses coefficient a to represent the degree of curvature. A single point calculation of Fe^{2+}-4N-GDQs adsorbed H_2 with a degree of curvature (a), i.e., -0.915 to 0.0915, was displayed in Figure 16. The H_2 adsorbed on Fe2+-4N-GDQs with various distances between Fe^{2+} and H_2 center from 2.5 Å to 4.0 Å at on-top sites were compared in **Table 4** and **Figure 17.** It was found that the curved Fe^{2+}-4N-GDQs can't adsorb H_2 at 2.5 Å. Although, almost curved Fe^{2+}-4N-GDQs prefer to adsorb H_2 at 3.0 Å, except the degree of curvature (a) of Fe^{2+}-4N-GDQs is 0.08139 and 0.0915, they prefer to adsorb H_2 at 3.5 Å. The H_2 adsorption energy is directly related to the positive degree of curvature, while the negative degree of curvature has a similar adsorption energy. Moreover, the H_2 adsorption energy on the outside (positive a value) of curved Fe^{2+}-4N-GDQs is greater than the inside (negative a value) of curved Fe^{2+}-4N-GDQs. We know that the curved Fe^{2+}-4N-GQDs could be modified for molecular H_2 adsorption, which can be applied for hydrogen gas storage.

จุฬาลงกรณ์มหาวิทยาลัย
CHULALONGKORN UNIVERSITY

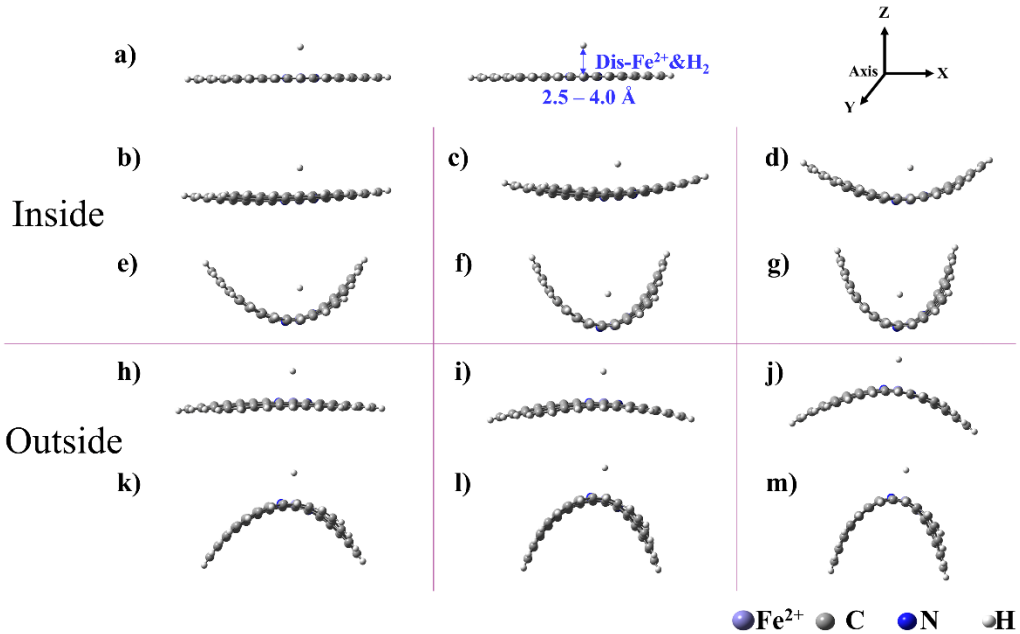

Figure 16 Side view single point calculation of Fe^{2+}-4N-GDQs adsorbed H^2 with various degrees of curvature, a) = 0, b) = -0.00728 c) = -0.01694, d) = -0.04018 e) = -0.06512, f) = -0.08139, g) = -0.0915, e) = 0.00728, f) = 0.01694, g) = -0.04018., k) = 0.06512, l) = 0.08139, m) = 0.0915.

จุฬาลงกรณ์มหาวิทยาลัย
CHULALONGKORN UNIVERSITY

Table 4 Adsorption energy, and distance between Fe^{2+} and H_2 center from 2.5 Å to 4.0 Å of Fe^{2+}-4N-GDQs adsorbed H_2 with different degrees of curvature (a).

Structure	(a)	Adsorption energy (kcal/mol)			
		2.5 Å	3.0 Å	3.5 Å	4.0 Å
(g)	-0.0915	1.47	-0.4	-0.51	-0.41
(f)	-0.0814	1.4	-0.39	-0.5	-0.4
(e)	-0.0651	1.44	-0.38	-0.49	-0.39
(d)	-0.0402	1.5	-0.4	-0.52	-0.4
(c)	-0.0169	1.03	-0.56	-0.57	-0.42
(b)	-0.0073	1.03	-0.61	-0.6	-0.43
(a)	0	1.04	-0.6	-0.6	-0.44
(h)	0.00728	1.06	-0.6	-0.6	-0.44
(i)	0.01694	1.1	-0.66	-0.65	-0.46
(j)	0.04018	1.54	-0.89	-0.91	-0.62
(k)	0.06512	2.74	-1.02	-1.28	-0.92
(l)	0.08139	1.55	-1.57	-1.53	-1
(m)	0.0915	0.98	-2.03	-1.9	-1.32

จุฬาลงกรณ์มหาวิทยาลัย
CHULALONGKORN UNIVERSITY

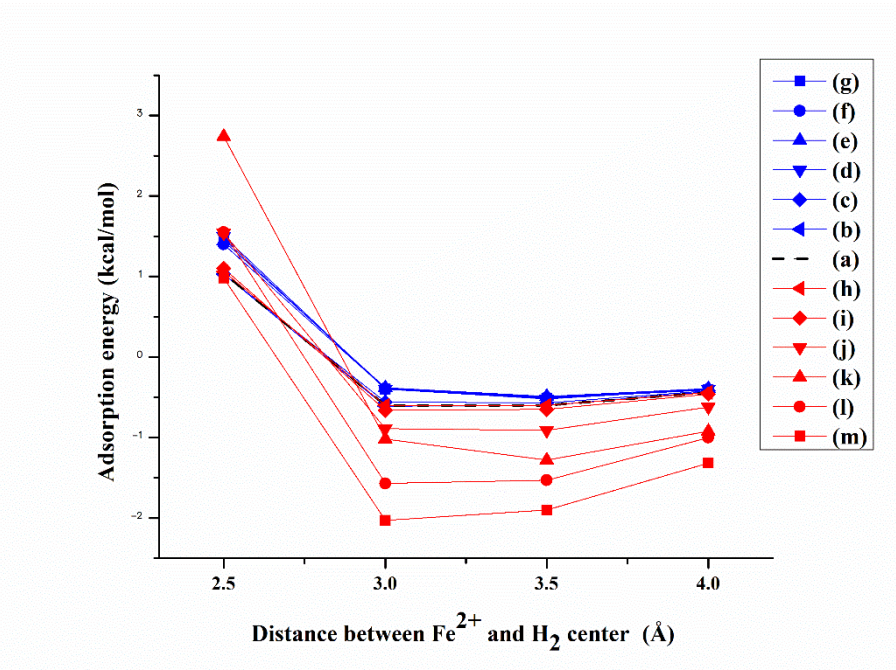

Figure 17 Adsorption energy, and distance between Fe^{2+} and H_2 center from 2.5 Å to 4.0 Å of Fe^{2+}-4N-GDQs adsorbed H_2 with different degrees of curvature (a)

จุฬาลงกรณ์มหาวิทยาลัย
CHULALONGKORN UNIVERSITY

CHAPTER V
CONCLUSION

In conclusion, we proposed a method to control curvature on GQDs and m-4N-GQDs by an external electric field performed with DFT calculation. The results demonstrate that the curved GQDs and m-4N-GQDs are directly related to the vertical electric field. The curvature of GQDs and m-4N-GQDs was curved in a concave and convex manner at positive and negative electric fields, respectively. It was found that the HOMO-LUMO gap of GQDs and m-4N-GQDs can be reduced when increasing the curvature. Therefore, the electronic properties of curved GQDs and m-4N-GQDs could be turned through EEFSs. Curved GQDs and m-4N-GQDs can be promising anchoring materials for semiconductors. We also found that the adsorption of molecular H_2 could be turned by the degree of curvature of Fe^{2+}-4N-GQDs. The molecular H_2 prefers to adsorb on the curved Fe^{2+}-4N-GQDs with on-top sites where the distance between Fe^{2+} and the H_2 center is 3.0–3.5 Å. The H_2 adsorption energy at the outside is stronger than at the inside of curved Fe^{2+}-4N-GQDs. The adsorption energy is based on the degree of curvature of Fe^{2+}-4N-GQDs with outside H_2 adsorption, while H_2 inside adsorption is slightly different. The curved Fe^{2+}-4N-GQDs could control molecular H_2 adsorption, which could be applied for hydrogen gas storage.

จุฬาลงกรณ์มหาวิทยาลัย
CHULALONGKORN UNIVERSITY

REFERENCES

1. Novoselov, K.; Geim, A.; Morozov, S.; Jiang, D.; Zhang, Y.; Dubonos, S.; Grigorieva, I.; Firsov, A., Electric field effect in atomically thin carbon films. *Science* **2004,** *306*, 666 - 669.

2. Yin, Z.; Zhu, J.; He, Q.; Cao, X.; Tan, C.; Chen, H.; Yan, Q.; Zhang, H., Graphene-Based Materials for Solar Cell Applications. *Advanced Energy Materials* **2014,** *4* (1), 1300574.

3. Sato, S., Graphene for nanoelectronics. *Japanese Journal of Applied Physics* **2015,** *54* (4), 040102.

4. Balog, R.; Jørgensen, B.; Nilsson, L.; Andersen, M.; Rienks, E.; Bianchi, M.; Fanetti, M.; Lægsgaard, E.; Baraldi, A.; Lizzit, S.; Sljivancanin, Z.; Besenbacher, F.; Hammer, B.; Pedersen, T. G.; Hofmann, P.; Hornekær, L., Bandgap opening in graphene induced by patterned hydrogen adsorption. *Nature Materials* **2010,** *9* (4), 315-319.

5. Welch, C. M.; Compton, R. G., The use of nanoparticles in electroanalysis: a review. *Analytical and Bioanalytical Chemistry* **2006,** *384* (3), 601-619.

6. Mérian, J.; Gravier, J.; Navarro, F.; Texier, I. Fluorescent nanoprobes dedicated to in vivo imaging: from preclinical validations to clinical translation *Molecules* [Online], 2012, p. 5564-5591.

7. Chen, H.; Wang, Z.; Zong, S.; Chen, P.; Zhu, D.; Wu, L.; Cui, Y., A graphene quantum dot-based FRET system for nuclear-targeted and real-time monitoring of drug delivery. *Nanoscale* **2015,** *7* (37), 15477-15486.

8. Lim, S. Y.; Shen, W.; Gao, Z., Carbon quantum dots and their applications. *Chemical Society Reviews* **2015,** *44* (1), 362-381.

9. Zhang, D.; Wen, L.; Huang, R.; Wang, H.; Hu, X.; Xing, D., Mitochondrial specific photodynamic therapy by rare-earth nanoparticles mediated near-infrared graphene quantum dots. *Biomaterials* **2018,** *153*, 14-26.

10. Li, M.; Chen, T.; Gooding, J. J.; Liu, J., Review of Carbon and Graphene Quantum Dots for Sensing. *ACS Sensors* **2019,** *4* (7), 1732-1748.

11. Zhang, X.; Wei, C.; Li, Y.; Yu, D., Shining luminescent graphene quantum dots:

จุฬาลงกรณ์มหาวิทยาลัย
CHULALONGKORN UNIVERSITY

Synthesis, physicochemical properties, and biomedical applications. *TrAC Trends in Analytical Chemistry* **2019,** *116*, 109-121.

12. Chung, H.-C.; Chang, C.-P.; Lin, C.-Y.; Lin, M.-F., Electronic and optical properties of graphene nanoribbons in external fields. *Physical Chemistry Chemical Physics* **2016,** *18* (11), 7573-7616.

13. Kistanov, A. A.; Cai, Y.; Zhou, K.; Dmitriev, S. V.; Zhang, Y.-W., Large Electronic Anisotropy and Enhanced Chemical Activity of Highly Rippled Phosphorene. *The Journal of Physical Chemistry C* **2016,** *120* (12), 6876-6884.

14. Cariglia, M.; Giambò, R.; Perali, A., Curvature-tuned electronic properties of bilayer graphene in an effective four-dimensional spacetime. *Physical Review B* **2017,** *95* (24), 245426.

15. Chang, S.-L.; Wu, B.-R.; Yang, P.-H.; Lin, M.-F., Geometric, magnetic and electronic properties of folded graphene nanoribbons. *RSC Advances* **2016,** *6* (69), 64852-64860.

16. Castro-Villarreal, P.; Ruiz-Sánchez, R., Pseudomagnetic field in curved graphene. *Physical Review B* **2017,** *95* (12), 125432.

17. Chang, S.-L.; Wu, B.-R.; Yang, P.-H.; Lin, M.-F., Curvature effects on electronic properties of armchair graphene nanoribbons without passivation. *Physical Chemistry Chemical Physics* **2012,** *14* (47), 16409-16414.

18. Pattarapongdilok, N.; Parasuk, V., Theoretical study on electronic properties of curved graphene quantum dots. *Computational and Theoretical Chemistry* **2018,** *1140*, 86-97.

19. Schniepp, H. C.; Kudin, K. N.; Li, J.-L.; Prud'homme, R. K.; Car, R.; Saville, D. A.; Aksay, I. A., Bending Properties of Single Functionalized Graphene Sheets Probed by Atomic Force Microscopy. *ACS Nano* **2008,** *2* (12), 2577-2584.

20. Xu, K.; Cao, P.; Heath, J. R., Scanning Tunneling Microscopy Characterization of the Electrical Properties of Wrinkles in Exfoliated Graphene Monolayers. *Nano Letters* **2009,** *9* (12), 4446-4451.

21. Schniepp, H. C.; Li, J.-L.; McAllister, M. J.; Sai, H.; Herrera-Alonso, M.; Adamson, D. H.; Prud'homme, R. K.; Car, R.; Saville, D. A.; Aksay, I. A., Functionalized Single Graphene Sheets Derived from Splitting Graphite Oxide. *The Journal of Physical Chemistry B* **2006,** *110* (17), 8535-8539.

จุฬาลงกรณ์มหาวิทยาลัย
CHULALONGKORN UNIVERSITY

22. Hallam, T.; Shakouri, A.; Poliani, E.; Rooney, A. P.; Ivanov, I.; Potie, A.; Taylor, H. K.; Bonn, M.; Turchinovich, D.; Haigh, S. J.; Maultzsch, J.; Duesberg, G. S., Controlled folding of graphene: GraFold printing. *Nano letters* **2015,** *15* (2), 857-863.

23. Bao, W.; Miao, F.; Chen, Z.; Zhang, H.; Jang, W.; Dames, C.; Lau, C. N., Controlled ripple texturing of suspended graphene and ultrathin graphite membranes. *Nature Nanotechnology* **2009,** *4* (9), 562-566.

24. Georgiou, T.; Britnell, L.; Blake, P.; Gorbachev, R. V.; Gholinia, A.; Geim, A. K.; Casiraghi, C.; Novoselov, K. S., Graphene bubbles with controllable curvature. *Applied Physics Letters* **2011,** *99* (9), 093103.

25. Zhang, Z.; Liu, B.; Hwang, K.-C.; Gao, H., Surface-adsorption-induced bending behaviors of graphene nanoribbons. *Applied Physics Letters* **2011,** *98* (12), 121909.

26. Ma, J.; Alfè, D.; Michaelides, A.; Wang, E., Stone-Wales defects in graphene and other planar $s{p}^{2}$-bonded materials. *Physical Review B* **2009,** *80* (3), 033407.

27. Meyer, J. C.; Kisielowski, C.; Erni, R.; Rossell, M. D.; Crommie, M. F.; Zettl, A., Direct Imaging of Lattice Atoms and Topological Defects in Graphene Membranes. *Nano Letters* **2008,** *8* (11), 3582-3586.

28. Banhart, F.; Kotakoski, J.; Krasheninnikov, A. V., Structural Defects in Graphene. *ACS Nano* **2011,** *5* (1), 26-41.

29. Cheng, M.; Yang, R.; Zhang, L.; Shi, Z.; Yang, W.; Wang, D.; Xie, G.; Shi, D.; Zhang, G., Restoration of graphene from graphene oxide by defect repair. *Carbon* **2012,** *50* (7), 2581-2587.

30. Ci, L.; Song, L.; Jin, C.; Jariwala, D.; Wu, D.; Li, Y.; Srivastava, A.; Wang, Z. F.; Storr, K.; Balicas, L.; Liu, F.; Ajayan, P. M., Atomic layers of hybridized boron nitride and graphene domains. *Nature Materials* **2010,** *9* (5), 430-435.

31. Wang, Y.; Shao, Y.; Matson, D. W.; Li, J.; Lin, Y., Nitrogen-Doped Graphene and Its Application in Electrochemical Biosensing. *ACS Nano* **2010,** *4* (4), 1790-1798.

32. Cortés-Arriagada, D.; Villegas-Escobar, N.; Ortega, D. E., Fe-doped graphene nanosheet as an adsorption platform of harmful gas molecules (CO, CO_2, SO_2 and H_2S), and the co-adsorption in O_2 environments. *Applied Surface Science* **2018,** *427*, 227-236.

33. Wang, Q.; Ji, Y.; Lei, Y.; Wang, Y.; Wang, Y.; Li, Y.; Wang, S., Pyridinic-N-Dominated Doped Defective Graphene as a Superior Oxygen Electrocatalyst for Ultrahigh-Energy-

จุฬาลงกรณ์มหาวิทยาลัย
CHULALONGKORN UNIVERSITY

Density Zn–Air Batteries. *ACS Energy Letters* **2018,** *3* (5), 1183-1191.

34. Mahendran, M.; Rekha, B.; Seenithurai, S.; Kodi Pandyan, R.; Vinodh Kumar, S., Hydrogen storage in Beryllium decorated graphene with double vacancy and porphyrin defect — A first principles study. *Functional Materials Letters* **2017,** *10* (03), 1750023.

35. Sarau, G.; Heilmann, M.; Bashouti, M.; Latzel, M.; Tessarek, C.; Christiansen, S., Efficient Nitrogen Doping of Single-Layer Graphene Accompanied by Negligible Defect Generation for Integration into Hybrid Semiconductor Heterostructures. *ACS Applied Materials & Interfaces* **2017,** *9* (11), 10003-10011.

36. Myradalyyev, S.; Limpanuparb, T.; Wang, X.; Hirao, H., Comparative computational analysis of binding energies between several divalent first-row transition metals (Cr^{2+}, Mn^{2+}, Fe^{2+}, Co^{2+}, Ni^{2+}, and Cu^{2+}) and ligands (porphine, corrin, and TMC). *Polyhedron* **2013,** *52*, 96-101.

37. Mombrú, D.; Romero, M.; Faccio, R.; Mombrú, A. W., Curvature and vacancies in graphene quantum dots. *Applied Surface Science* **2018,** *462*, 540-548.

38. Padilha, J. E.; Amorim, R. G.; Rocha, A. R.; da Silva, A. J. R.; Fazzio, A., Energetics and stability of vacancies in carbon nanotubes. *Solid State Communications* **2011,** *151* (6), 482-486.

39. Bodrenko, I. V.; Avdeenkov, A. V.; Bessarabov, D. G.; Bibikov, A. V.; Nikolaev, A. V.; Taran, M. D.; Tkalya, E. V., Hydrogen Storage in Aromatic Carbon Ring Based Molecular Materials Decorated with Alkali or Alkali-Earth Metals. *The Journal of Physical Chemistry C* **2012,** *116* (48), 25286-25292.

40. Zhang, Y.; Cui, H.; Tian, W.; Liu, T.; Wang, Y., Effect of hydrogen adsorption energy on the electronic and optical properties of Si-modified single-layer graphene with an Al decoration. *AIP Advances* **2020,** *10* (4), 045012.

41. Cui, H.; Zhang, Y.; Tian, W.; Wang, Y.; Liu, T.; Chen, Y.; Shan, P.; Yuan, H., A study on hydrogen storage performance of Ti decorated vacancies graphene structure on the first principle. *RSC Advances* **2021,** *11* (23), 13912-13918.

42. Haldar, S.; Mukherjee, S.; Singh, C. V., Hydrogen storage in Li, Na and Ca decorated and defective borophene: a first principles study. *RSC Advances* **2018,** *8* (37), 20748-20757.

43. Celik, F. A., Hydrogen adsorption and storage behaviors of Li-decorated PdS2

จุฬาลงกรณ์มหาวิทยาลัย
Chulalongkorn University

monolayer: An extended tight-binding study based on DFT. *International Journal of Hydrogen Energy* **2022**.

44. Zhou, Y.; Chu, W.; Jing, F.; Zheng, J.; Sun, W.; Xue, Y., Enhanced hydrogen storage on Li-doped defective graphene with B substitution: A DFT study. *Applied Surface Science* **2017,** *410*, 166-176.

45. Rasmussen, J. J.; Rypdal, K., Blow-up in Nonlinear Schroedinger Equations-I A General Review. *Physica Scripta* **1986,** *33* (6), 481.

46. Roothaan, C. C. J., New Developments in Molecular Orbital Theory. *Reviews of Modern Physics* **1951,** *23* (2), 69-89.

47. Hall, G. G., The Molecular Orbital Theory of Chemical Valency. VIII. A Method of Calculating Ionization Potentials. *Proceedings of the Royal Society of London A: Mathematical, Physical and Engineering Sciences* **1951,** *205* (1083), 541-552.

48. Lundqvist, S.; March, N. H., *Theory of the inhomogeneous electron gas*. Plenum Press: New York, 1983; p xiii, 395 p.

49. Cramer, C. J.; Truhlar, D. G., Density functional theory for transition metals and transition metal chemistry. *Physical Chemistry Chemical Physics* **2009,** *11* (46), 10757-10816.

50. Deutschmann, O., *Modeling and simulation of heterogeneous catalytic reactions: from the molecular process to the technical system*. John Wiley & Sons: 2013.

51. Slater, J. C., The Theory of Complex Spectra. *Physical Review* **1929,** *34* (10), 1293-1322.

52. Schlegel, H. B.; Frisch, M. J., Transformation between Cartesian and pure spherical harmonic Gaussians. *Int J Quantum Chem* **1995,** *54* (2), 83-87.

53. Frisch, M. J.; Trucks, G. W.; Schlegel, H. B.; Scuseria, G. E.; Robb, M. A.; Cheeseman, J. R.; Scalmani, G.; Barone, V.; Petersson, G. A.; Nakatsuji, H.; Li, X.; Caricato, M.; Marenich, A.; Bloino, J.; Janesko, B. G.; Gomperts, R.; Mennucci, B.; Hratchian, H. P.; Ortiz, J. V.; Izmaylov, A. F.; Sonnenberg, J. L.; Williams-Young, D.; F. Ding, F. L.; F. Egidi, J. G.; B. Peng, A. P.; Henderson, T.; Ranasinghe, D.; Zakrzewski, V. G.; J. Gao, N. R., G. Zheng; W. Liang, M. H., M. Ehara; K. Toyota, R. F., J. Hasegawa ; M. Ishida, T. N.; Y. Honda, O. K., H. Nakai; T. Vreven, K. T.; Montgomery, J. A.; Jr., J. E. P.; F. Ogliaro, M. B.; J.

จุฬาลงกรณ์มหาวิทยาลัย
Chulalongkorn University

J. Heyd, E. B.; K. N. Kudin, V. N. S.; T. Keith, R. K.; Normand, J.; Raghavachari, K.; Rendell, A.; Burant, J. C.; Iyengar, S. S.; J. Tomasi, M. C.; J. M. Millam, M. K.; C. Adamo, R. C.; Ochterski, J. W.; R. L. Martin, K. M.; Farkas, O.; Foresman, J. B.; Fox, D. J., Gaussian 09,Revision D.01. Gaussian, Inc., Wallingford CT, 2009.

54. Kuamit, T.; Ratanasak, M.; Rungnim, C.; Parasuk, V., Effects of shape, size, and pyrene doping on electronic properties of graphene nanoflakes. *Journal of Molecular Modeling* **2017,** *23* (12), 355.

จุฬาลงกรณ์มหาวิทยาลัย
CHULALONGKORN UNIVERSITY

APPENDIX

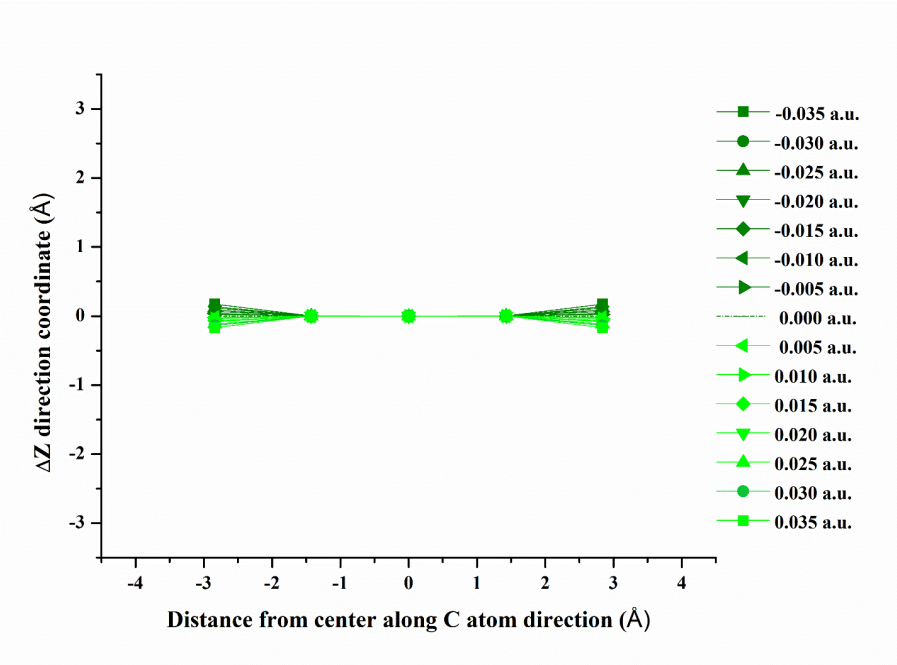

Figure A1 Plot of Z coordinate variations (ΔZ) and distance from in Å along C atom direction for $C_{24}H_{12}$ at various external electric fields from -0.035 to +0.035 a.u..

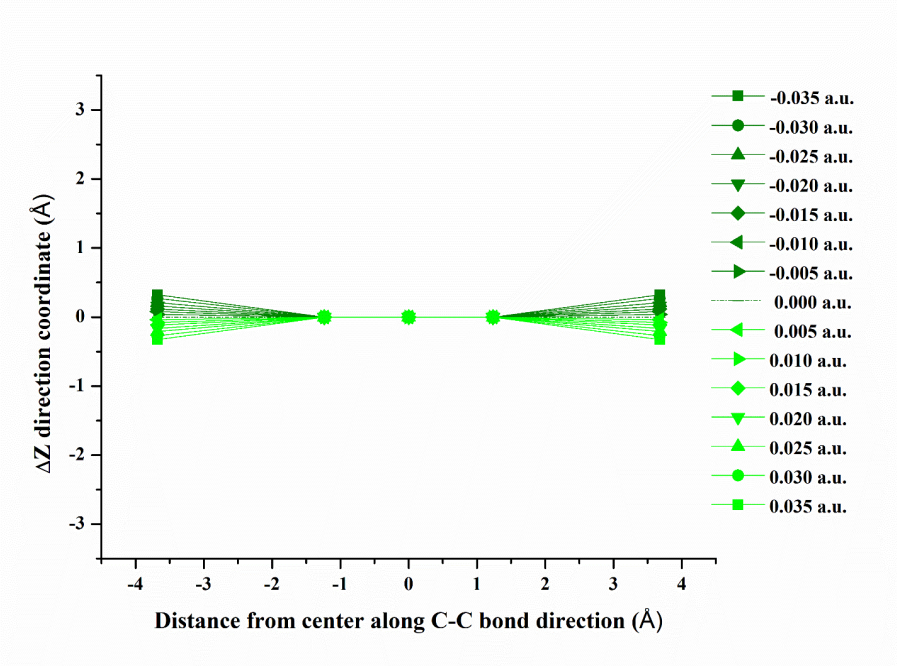

Figure A2 Plot of Z coordinate variations (ΔZ) and distance from in Å along C-C bond direction for $C_{24}H_{12}$ at various external electric fields from -0.035 to +0.035 a.u..

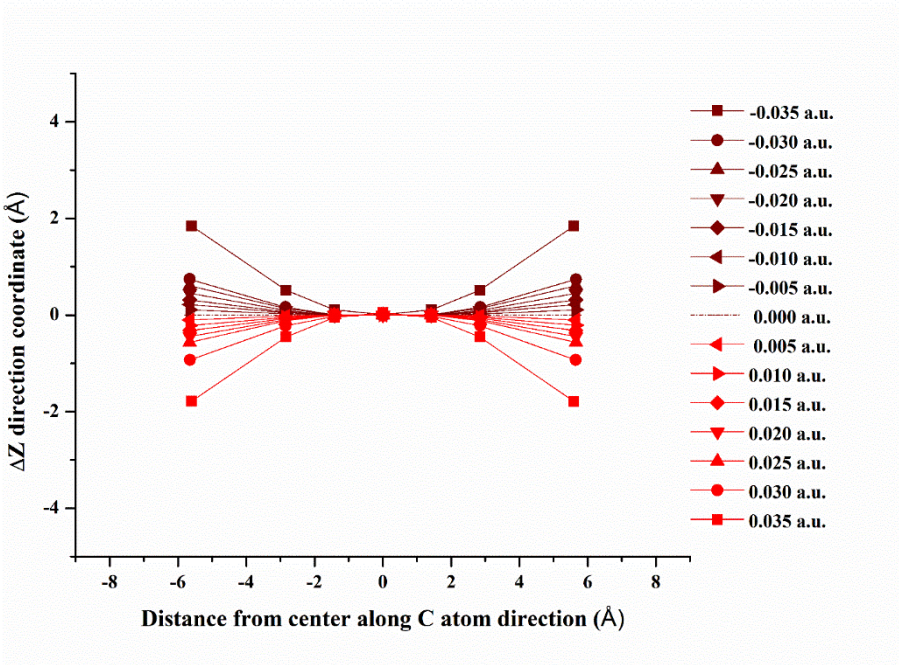

Figure A3 Plot of Z coordinate variations (ΔZ) and distance from in Å along C atom direction for $C_{54}H_{18}$ at various external electric fields from -0.035 to +0.035 a.u..

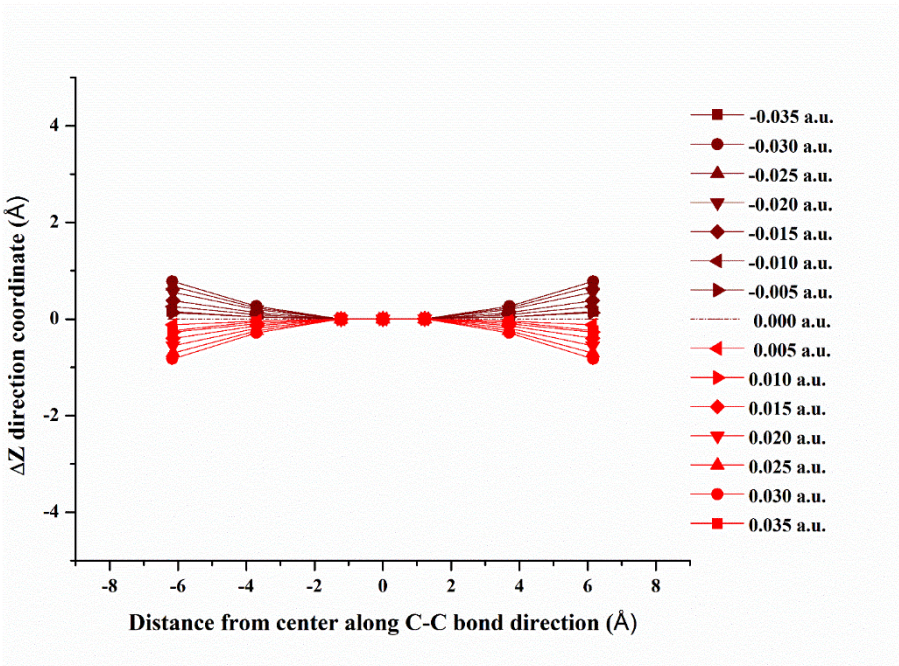

Figure A4 Plot of Z coordinate variations (ΔZ) and distance from in Å along C-C bond direction for $C_{54}H_{18}$ at various external electric fields from -0.035 to +0.035 a.u..

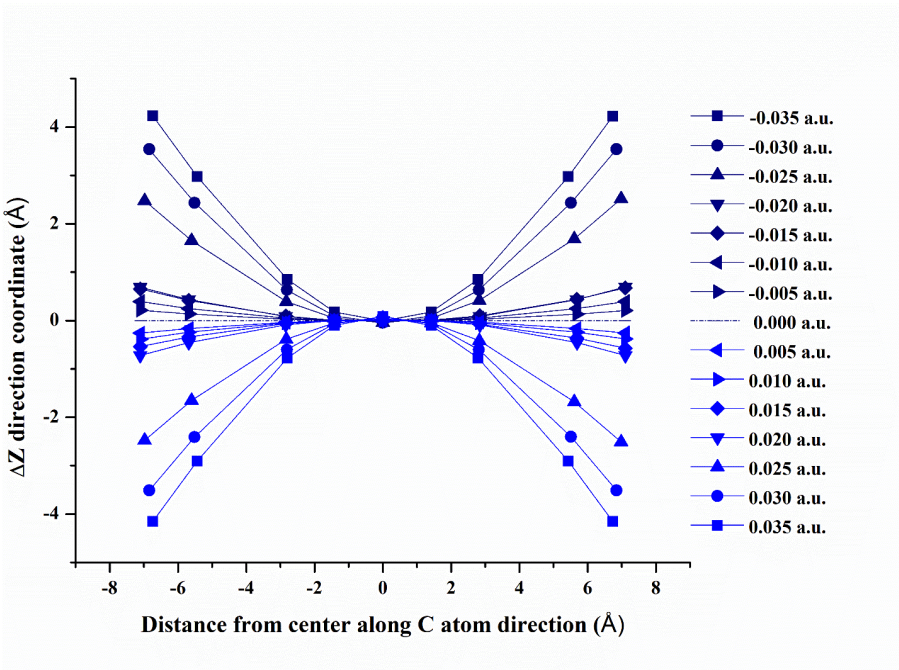

Figure A5 Plot of Z coordinate variations (ΔZ) and distance from in Å along C atom direction for $C_{96}H_{24}$ at various external electric fields from -0.035 to +0.035 a.u..

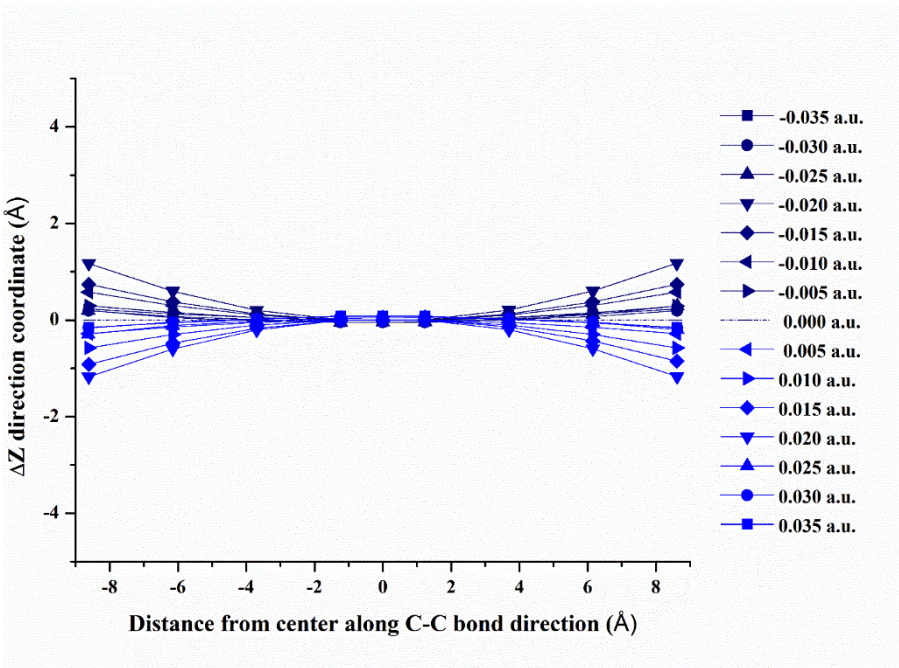

Figure A6 Plot of Z coordinate variations (ΔZ) and distance from in Å along C-C bond direction for $C_{96}H_{24}$ at various external electric fields from -0.035 to +0.035 a.u..

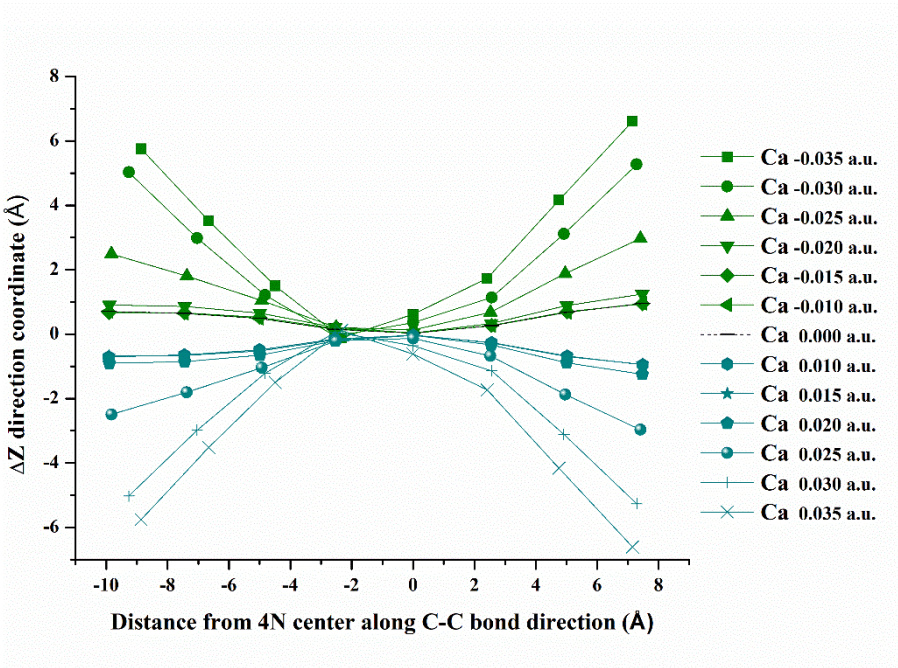

Figure A7 Plot of Z coordinate variations (ΔZ) and distance from in Å along C-C bond direction for Ca-4N-GQDs at various external electric fields from -0.035 to +0.035 a.u.

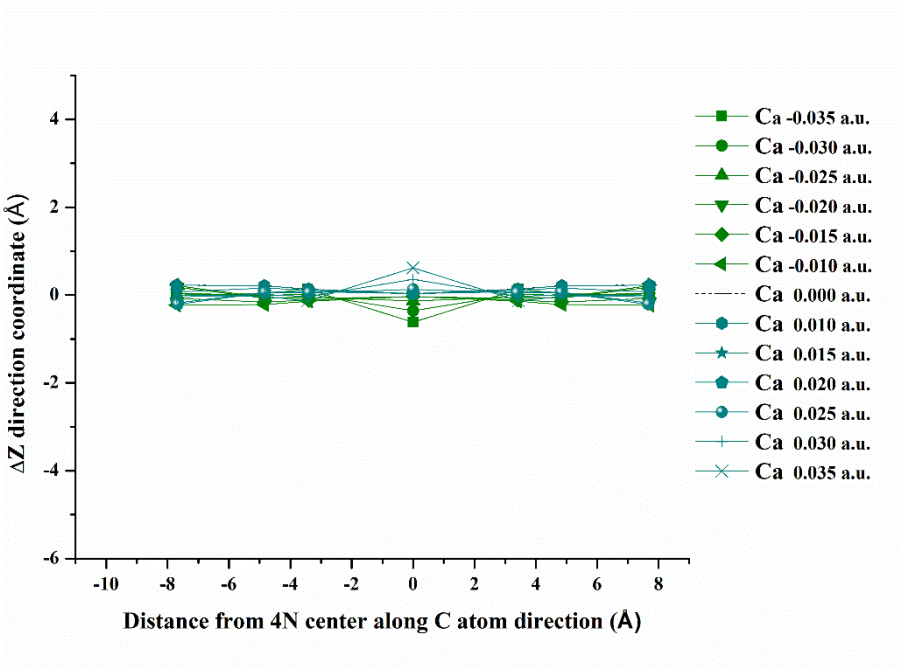

Figure A8 Plot of Z coordinate variations (ΔZ) and distance from in Å along C atom direction for Ca-4N-GQDs at various external electric fields from -0.035 to +0.035 a.u.

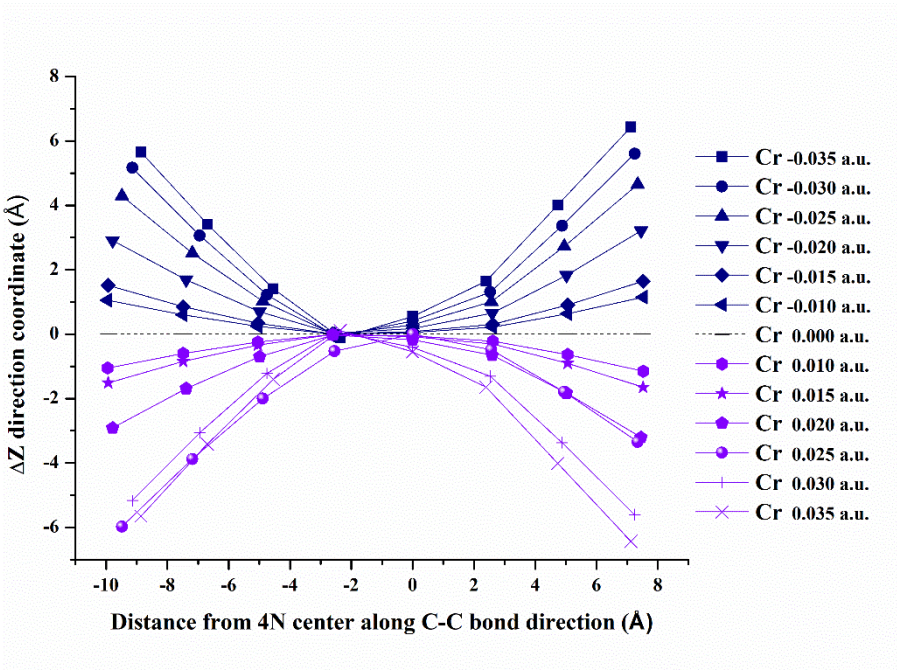

Figure A9 Plot of Z coordinate variations (ΔZ) and distance from in Å along C-C bond direction for Cr-4N-GQDs at various external electric fields from -0.035 to +0.035 a.u.

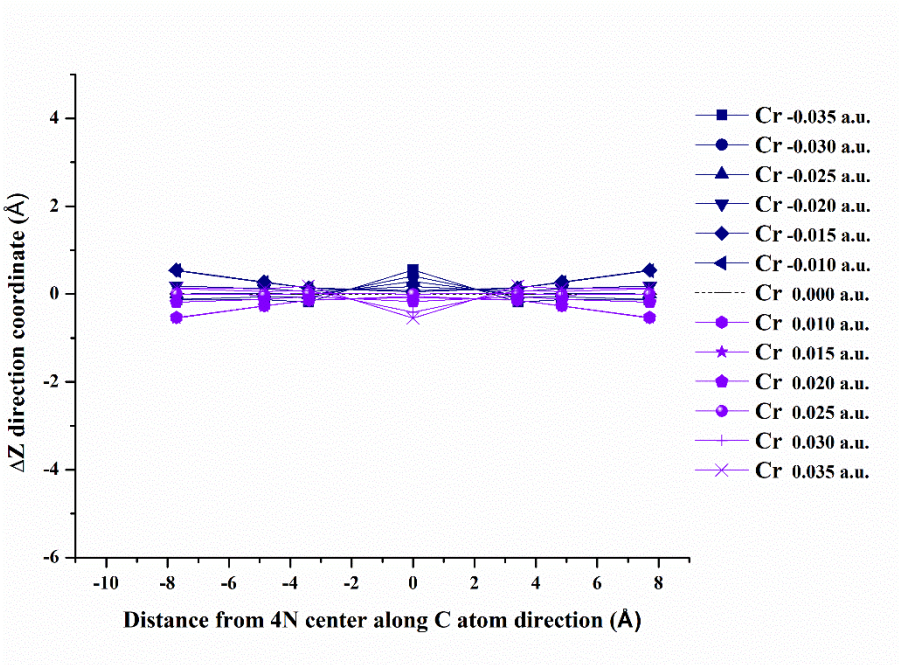

Figure A10 Plot of Z coordinate variations (ΔZ) and distance from in Å along C atom direction for Cr-4N-GQDs at various external electric fields from -0.035 to +0.035 a.u.

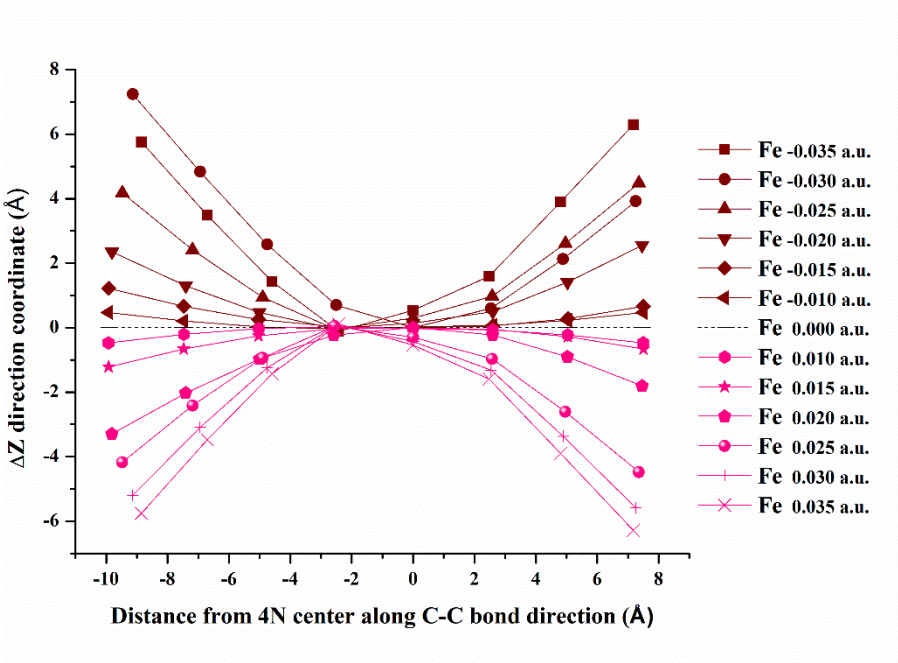

Figure A11 Plot of Z coordinate variations (ΔZ) and distance from in Å along C-C bond direction for Fe-4N-GQDs at various external electric fields from -0.035 to +0.035 a.u.

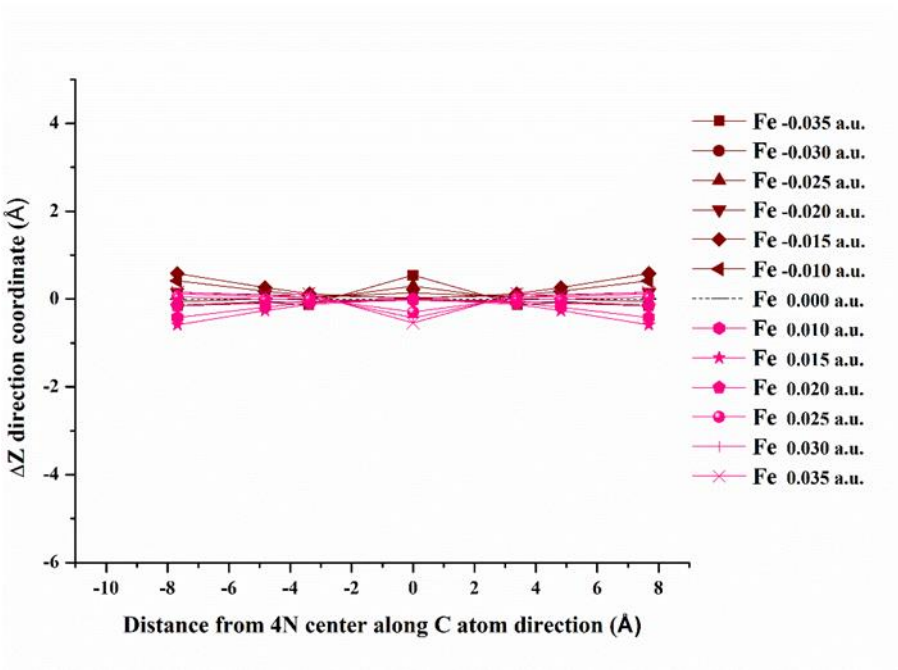

Figure A12 Plot of Z coordinate variations (ΔZ) and distance from in Å along C atom direction for Fe-4N-GQDs at various external electric fields from -0.035 to +0.035 a.u.

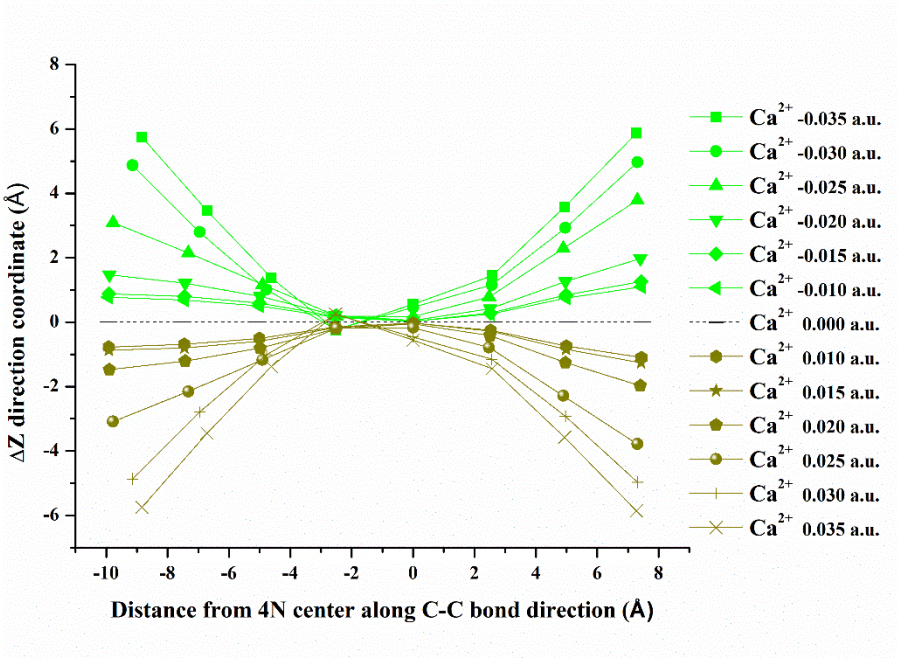

Figure A13 Plot of Z coordinate variations (ΔZ) and distance from in Å along C-C bond direction for Ca^{2+}-4N-GQDs at various external electric fields from -0.035 to +0.035 a.u.

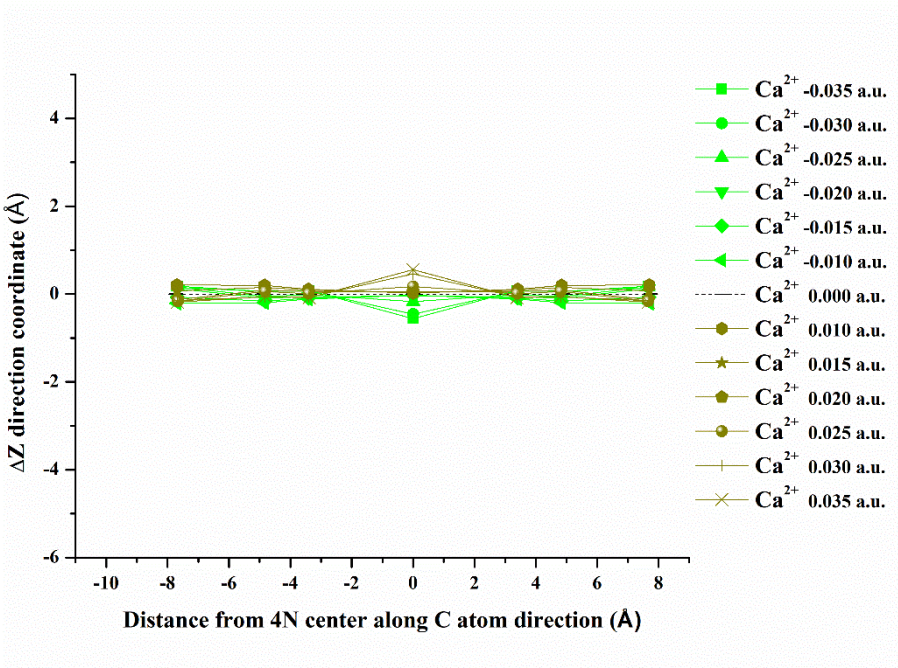

Figure A14 Plot of Z coordinate variations (ΔZ) and distance from in Å along C atom direction for Ca^{2+}-4N-GQDs at various external electric fields from -0.035 to +0.035 a.u.

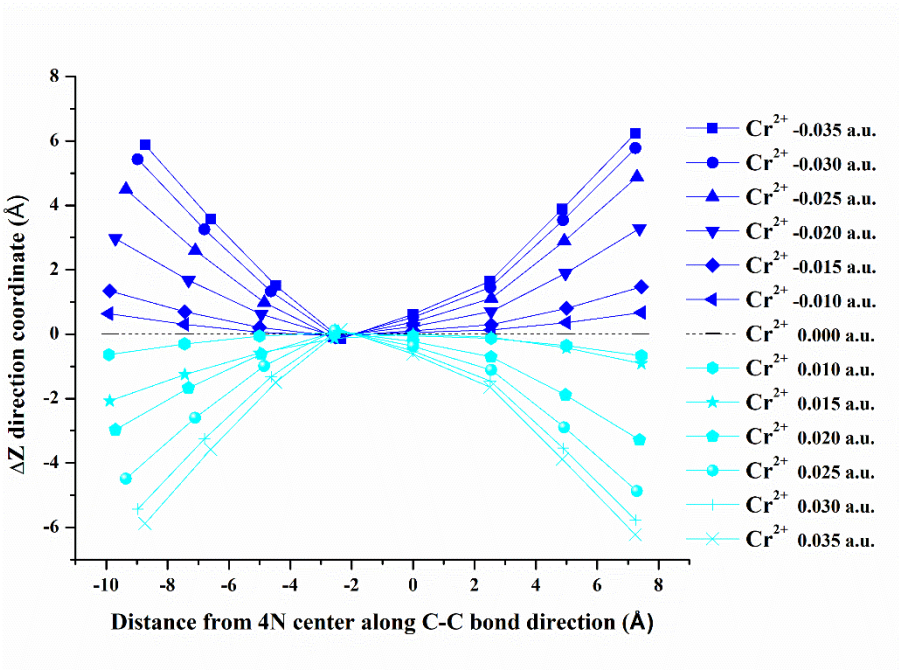

Figure A15 Plot of Z coordinate variations (ΔZ) and distance from in Å along C atom direction for Cr^{2+} 4N-GQDs at various external electric fields from -0.035 to +0.035 a.u.

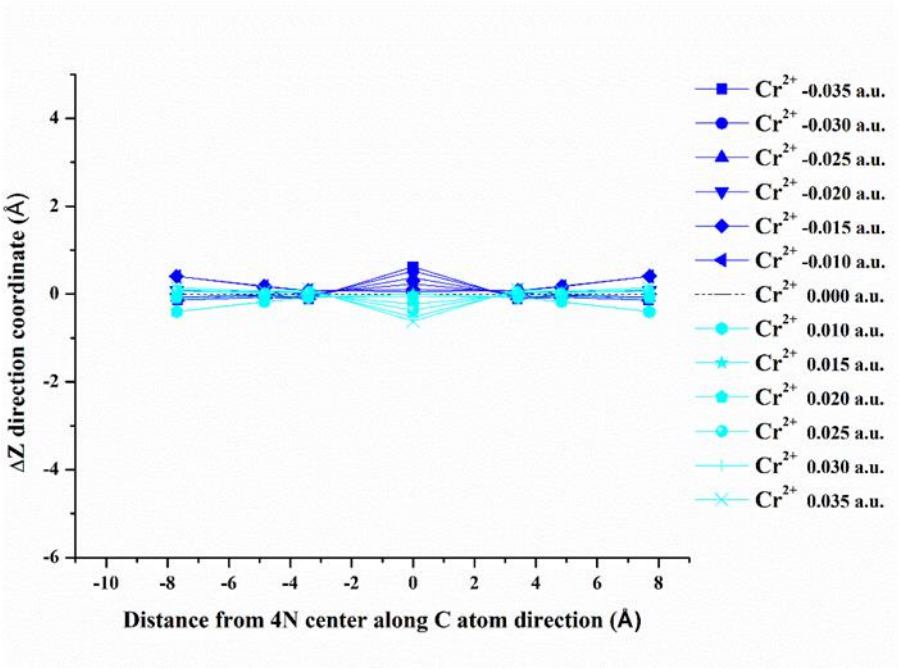

Figure A16 Plot of Z coordinate variations (ΔZ) and distance from in Å along C atom direction for Cr^{2+}-4N-GQDs at various external electric fields from -0.035 to +0.035 a.u.

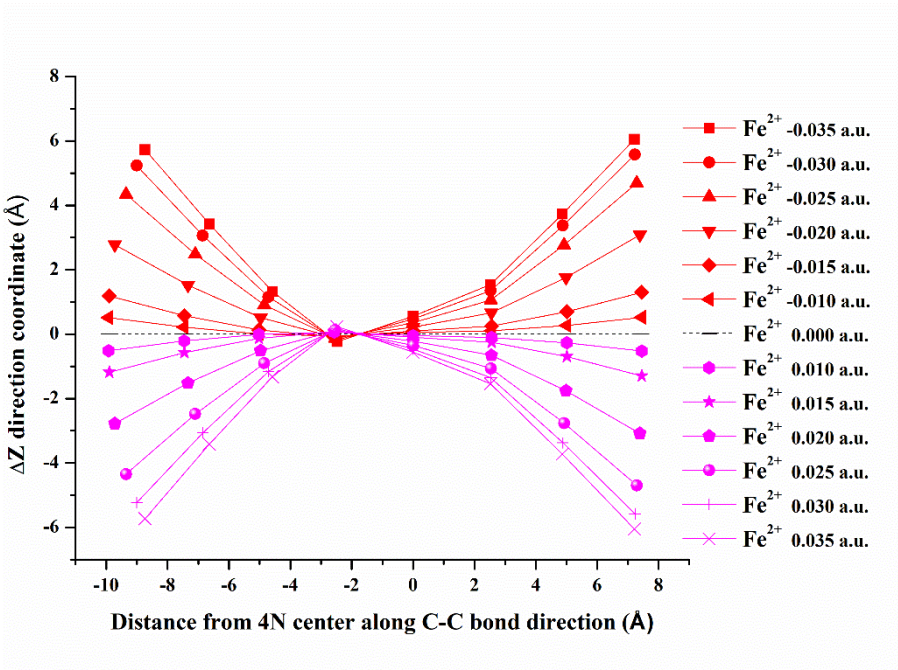

Figure A17 Plot of Z coordinate variations (ΔZ) and distance from in Å along C atom direction for Fe^{2+}-4N-GQDs at various external electric fields from -0.035 to +0.035 a.u.

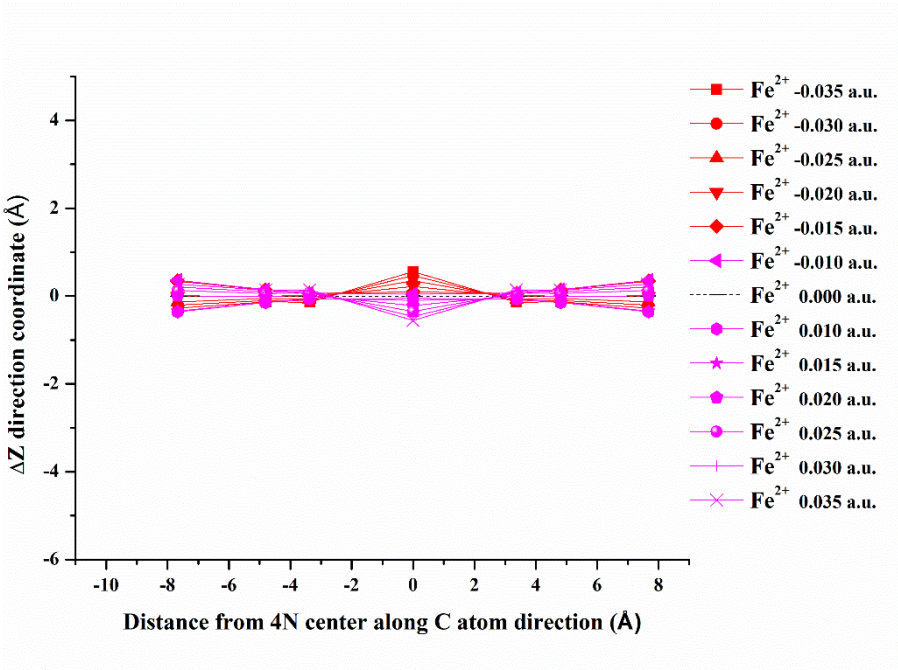

Figure A18 Plot of Z coordinate variations (ΔZ) and distance from in Å along C atom direction for Fe^{2+}-4N-GQDs at various external electric fields from -0.035 to +0.035 a.u.

VITA

NAME	Thanawit Kuamit
DATE OF BIRTH	17 April 1990
PLACE OF BIRTH	Phatthalung
INSTITUTIONS ATTENDED	Chulalongkorn University
HOME ADDRESS	454/104 Phetchaburi 7 Alley, Thung Phaya Thai, Ratchathewi, Bangkok 10400
PUBLICATION	1. Kuamit, T.; Ratanasak, M.; Rungnim, C.; Parasuk, V., Effects of shape, size, and pyrene doping on electronic properties of graphene nanoflakes. Journal of Molecular Modeling 2017, 23 (12), 355.

จุฬาลงกรณ์มหาวิทยาลัย
CHULALONGKORN UNIVERSITY